

Characteristics and prediction methods for tunnel deformations induced by excavations

Gang Zheng^{1,2}, Yiming Du^{1,2}, Xuesong Cheng^{*1,2},
Yu Diao^{1,2}, Xu Deng^{1,2} and Fanjun Wang^{1,2}

¹MOE Key Laboratory of Coast Civil Structure Safety, Tianjin University,
92 Weijin Rd., Nankai District, Tianjin 300072, China

²Department of Civil Engineering, Tianjin University,
92 Weijin Rd., Nankai District, Tianjin 300072, China

(Received March 09, 2016, Revised October 13, 2016, Accepted November 22, 2016)

Abstract. The unloading effect from excavations can cause the deformation of adjacent tunnels, which may seriously influence the operation and safety of those tunnels. However, systematic studies of the deformation characteristics of tunnels located along side excavations are limited, and simplified methods to predict the influence of excavations on tunnels are also rare. In this study, the simulation capability of a finite element method (FEM) considering the small-strain characteristics of soil was verified using a case study. Then, a large number of FEM simulations examining the influence of excavations on adjacent tunnels were conducted. Based on the simulation results, the deformation characteristics of tunnels at different positions and under four deformation modes of the retaining structure were analyzed. The results indicate that the deformation mode of the retaining structure has a significant influence on the deformation of certain tunnels. When the deformation magnitudes of the retaining structures are the same, the influence degree of the excavation on the tunnel increased in this order: from cantilever type to convex type to composite type to kick-in type. In practical projects, the deformation mode of the retaining structure should be optimized according to the tunnel position, and kick-in deformation should be avoided. Furthermore, two methods to predict the influence of excavations on adjacent tunnels are proposed. Design charts, in terms of normalized tunnel deformation contours, can be used to quantitatively estimate the tunnel deformation. The design table of the excavation influence zones can be applied to determine which influence zone the tunnel is located in.

Keywords: deep excavation; tunnel; influence zone; deformation mode; prediction method

1. Introduction

With the continuous development of urban rail transport systems, a larger number of tunnels have been constructed and put into operation. The tunnels in operation are susceptible to surrounding construction activities (Bousbia and Messast 2015, Do *et al.* 2014). However, due to the increasing demand for infrastructure in congested urban cities, underground construction, including deep excavation, has become commonplace. These excavations can cause stress changes and soil deformation in the ground, which may in turn induce remarkable deformation in existing

*Corresponding author, Ph.D., E-mail: cheng_xuesong@163.com

adjacent tunnels and even affect the safety and serviceability of these tunnels.

In practical engineering, an existing tunnel may be located directly beneath an excavation or to the side of an excavation. When the excavation is constructed directly above an existing tunnel, the tunnel will move upwards significantly due to the unloading effect of the overlying soil. Many

Table 1 Summary of excavation cases adjacent to existing tunnels

Case No.	Case name	Excavation depth H	Maximum horizontal displacement of the retaining structure δ_{hmax}	Information about the existing tunnel			Deformation of the existing tunnel ⁽¹⁾	
				Type	Buried depth	Distance from the wall	Horizontal displacement	Settlement
1	An excavation of a high-rise building in Taipei (Chang <i>et al.</i> 2001a)	21 m	53 mm	Metro	14.5 m	6.9 m	27 mm	-33 mm
2	New City World in Shanghai (Hu <i>et al.</i> 2003)	12.5 m	14.2 mm	Metro	7.4 m	3 m	9 mm	-5 mm
3	An excavation in Taipei (Hwang <i>et al.</i> 2011)	15.9 m	54 mm	Metro	16.1 m	7.3 m	50 mm (21.5 mm) ⁽²⁾	(-21.4 mm)
4	The diaphragm construction of an excavation in Taipei (Hwang <i>et al.</i> 2011)	Diaphragm wall construction	—	Metro	12.9 m	3 m	(17 mm)	(-2 mm)
5	Tan Tock Seng Hospital in Singapore (Sharma <i>et al.</i> 2001)	15 m	—	Metro	17 m	18 m	6.0 mm /4.0 mm ⁽³⁾	3.8 mm /2.1 mm
6	Jing An Si Station of Metro Line 7 in Shanghai	23.35 m	—	Metro	~8.5 m	15 m	3.2 mm	-1.3 mm
7	The excavation of a high-rise building in East China (Jiang and Zhang 2013)	7 m	—	Metro	10 m	4 m	1.4 mm	6.8 mm
8	The excavation of a square in Shanghai	14.4 m	—	Metro	~9.3 m	7-11 m	10 mm	-10 mm
9	The excavation of Shanghai Square (the northern pit)	~16 m	—	Metro	~14.4 m	2.8-5 m	13 mm	-5 mm
10	An excavation in the 1788 Plot in Shanghai (two tunnels)	~14 m	22 m	Metro	~8.5 m	10.4 m /27.5 m	—	2.85 mm /-2.4 mm
11	Hai Zhu City Plaza in Canton	21 m	—	Metro	14.5 m	5.7 m-6.6 m	6.9 mm	—
12	The building group on Huang Sha metro station in Canton	12 m	—	Metro	7 m	6 m	8 mm	-12.3 mm
13	Yu Nian International Business Building in Shanghai	~10 m	—	Metro	~7 m	7.2 m	4.8 mm	-3.3 mm
14	Hong Hui Tower in Canton	16.9 m	—	Metro	9.9 m	8.4 m	8.5 mm	—

Table 1 Summary of excavation cases adjacent to existing tunnels

Case No.	Case name	Excavation depth H	Maximum horizontal displacement of the retaining structure δ_{hmax}	Information about the existing tunnel			Deformation of the existing tunnel ⁽¹⁾	
				Type	Buried depth	Distance from the wall	Horizontal displacement	Settlement
15	Da Ning Commercial Center in the Zhabei district of Shanghai	6 m-6.7 m	20.7 mm	Metro	11.8 m	5.45 m	4 mm	7.1 mm
16	A building in Guangzhou	18 m	—	Metro (Box)	11 m	14.8 m	5.8 mm	-6.8 mm
17	An excavation in the Xuhui district of Shanghai	19.9 m	—	Metro	11 m	25 m	—	-5.54 mm
18	The No. 3 plot of Huaihai Zhong Road in Shanghai	13.85 m	6 mm	Metro	8.37 m	8 m	—	-5 mm
19	An excavation in Tianjin	15 m	50 mm	CRH	15 m	16.6 m	14.86 mm	7.44 mm
20	Shanghai Wheelock Square	18.02 m	—	Metro	8.5 m	5.4 m	—	-16.67 mm
21	A high-rise building in the Suzhou Industrial Park	12.2 m	—	Metro	11.4 m-12.7 m	9.5 m-14 m	1.05 mm	6.5 mm
22	A project in Hangzhou	~13 m	19.5 mm	Metro	7.3 m	8.1 m	1.52 mm	-4.11 mm
23	Malaysian Business Center in Guangzhou	—	—	Metro	—	—	3.5 mm	5 mm
24	An excavation in Singapore	8.2 m	—	Metro	~15 m	3.6 m	3.2 mm /1.9 mm	3.1 mm /1.6 mm
25	LuNeng Mansion in Tianjin	15.7 m	44.6 mm	Metro	13.3 m-15.2 m	10.3 m-15.2 m	8.89 mm	-5.9 mm

(1) The positive deformation values are horizontal displacements toward the excavation and the vertical upheaval displacement.

(2) The parenthesized values are tunnel diameter convergence values, and the positive values are the increments in the tunnel diameter.

(3) For the values of twin tunnels, the first value is the value of the tunnel closer to the excavation.

researchers have studied this phenomenon via field monitoring (Burford 1988, Doležalová 2001), centrifuge tests (Zheng *et al.* 2010, Ng *et al.* 2013, 2015b), numerical simulations (Ng *et al.* 2015a, Huang *et al.* 2014, 2011, Liu *et al.* 2011, Zheng and Wei 2008), and theoretical derivations (Zhang *et al.* 2013). Some researchers have noted that when the tunnel is situated next to an excavation,

the influence on the tunnel is smaller than that on an underlying tunnel (Liu *et al.* 2011, Ng *et al.* 2015b, Huang *et al.* 2011). However, there have been many cases where tunnels located next to excavations were damaged by excavations. For example, segments of a tunnel in the Taipei Rapid Transit System (TRTS) were cracked, and concrete slabs became detached from the segments due to adjacent excavation in November 1995 (Chang *et al.* 2001b, Hwang *et al.* 2011). Table 1 lists some cases in which existing tunnels were affected by adjacent excavations.

When an excavation is located next to an existing tunnel, because of the complex stress and displacement fields outside the excavation, the movement values and directions of the tunnel at different locations relative to the excavation are different. As shown in Table 1, although all tunnels moved toward the excavations in the horizontal direction, the vertical displacements of the tunnels could be upward or downward, which is different than the behavior of tunnels underlying excavations. As shown in Table 1, some tunnels (e.g., Case 1) experienced a settlement deformation, whereas others (e.g., Case 7) experienced a heave deformation. Table 1 indicates that the differences of numerous factors, such as the tunnel position relative to the excavation, excavation depth, deformation of the retaining structure, soil condition, and construction method, caused significant differences in the tunnel deformation.

The linings of the shield tunnels in operation are usually made of precast concrete segments connected by high-strength bolts, which are susceptible to deformation. Excess deformation can lead to cracking and dislocation of the segment joints and to detachment of the concrete slab from the segments (Chang *et al.* 2001a, Richards 1998), which may affect the train operation or even cause leakage of sand and water that can seriously damage the tunnel. Therefore, it is crucial to strictly control deformations of tunnels in operation.

To protect the existing tunnels, the total settlement and horizontal displacement should be less than 20 mm, as stipulated in “Technical management interim regulations of building constructions for the protection of the adjacent metro in Shanghai” (No. 854 of Shanghai Municipal Statute 1994, called “Shanghai regulations” for simplicity). This rule was proposed very early in China (in 1994); therefore, it has been widely applied in the soft clay areas of the coastal regions of China. In the last few years, national and industrial standards have been issued in China. The Alert Level and Action Level of the horizontal and vertical displacements of a tunnel were set at 10 mm and 20 mm, respectively, in the industry standard, “Technical code for protection structures of urban rail transit” (CJJ/T 202-2013). Stricter control criteria were proposed by the national standard, “Code for monitoring the measurement of urban rail transit engineering” (GB 50911-2013), in which the controlled values of the settlement, the upheave displacement, and the horizontal displacement of a tunnel were set at 3-10 mm, 5 mm, and 3-5 mm, respectively.

These strict deformation control rules create an urgent necessity to estimate the deformation of the adjacent tunnel and to propose the corresponding protective measures prior to the excavation.

Some researchers have studied the influence of excavation on existing tunnels located along side excavations. However, these studies usually focus on the characteristics of the deformation and the internal forces of the existing tunnel induced by the excavation based on a specific project (Chang *et al.* 2001a, Hwang *et al.* 2011, Hu *et al.* 2003, Sharma *et al.* 2001), whereas systematic and general principle studies of tunnel deformation induced by excavations are limited. Furthermore, simplified methods to predict tunnel deformation and evaluate the influence degree of the excavation on the tunnel have rarely been investigated.

When a tunnel is located next to an excavation, the tunnel deformation is directly related to the deformation of the retaining structure of the excavation. The deflection modes of the retaining structures can be divided into four types (Zheng and Li 2012), i.e., cantilever-type, convex-type,

composite-type, and kick-in-type, as shown in Fig. 1. Even in an excavation, the retaining piles at different locations can exhibit different deflection modes. In the codes, the deformation control rules of excavations usually restrict the maximum deformation of the retaining structure regardless of the deformation mode. However, Zheng and Li (2012) found that when the maximum deformations are the same but the deformation modes are different, the ground settlement and the deformation of buildings can differ remarkably. As a result, when the deformation modes of the retaining structures are different, the deformation of the adjacent tunnels can also be different. Therefore, the deformation mode should be considered in the analysis of the influence on the existing tunnel.

One method to evaluate the influence degree of an excavation on an existing tunnel is to sketch the influence zones of the excavation and determine which influence zone the tunnel is located in. In Shanghai regulations, construction activity is forbidden within 3 m of tunnels (No. 854 of Shanghai Municipal Statute 1994). Some standards have suggested the locations of influence zones for existing tunnels around excavations (GJJ/T 202-2013, GB 50911-2013, The British Tunneling Society 2006). However, these influence zones are primarily related to the distance between the excavation and the tunnel. The influences of the deformation modes, the magnitude of the retaining structures, and the control criterion of the tunnel deformation were not considered in the partition methods of the influence zones proposed by the above standards. More specific influence zones, which can be used to predict tunnel deformation or the influence degree of an excavation on a tunnel, still need to be investigated.

In this study, an excavation project in Tianjin, which was close to an existing tunnel, was taken as a case study in which the displacements of the diaphragm wall, the soil outside the excavation,

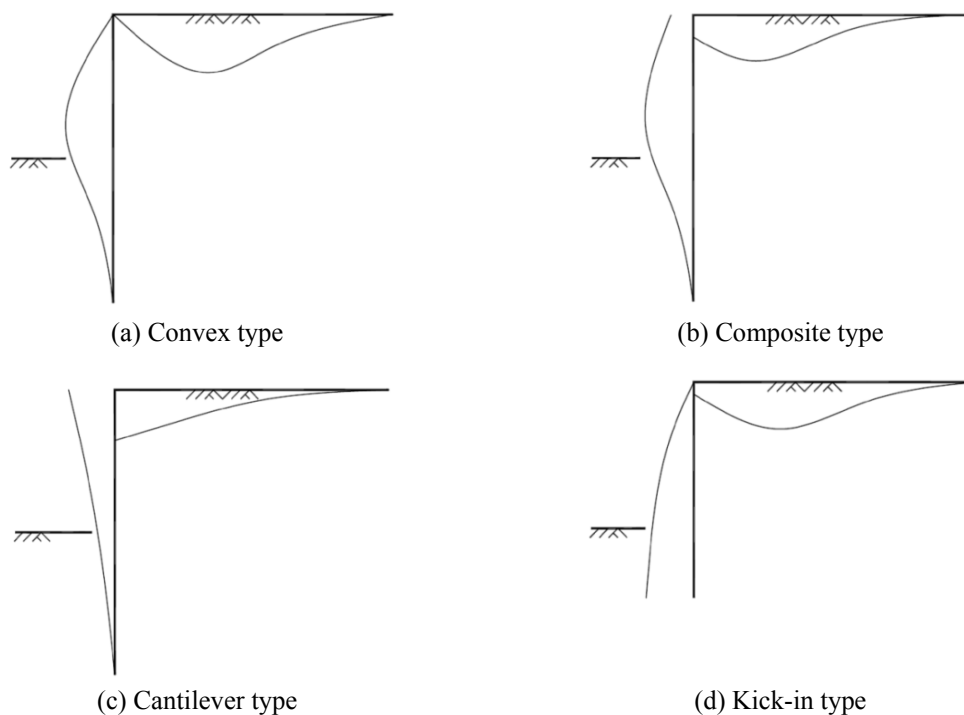


Fig. 1 Typical profiles of retaining structure deflection modes (Zheng and Li 2012)

and the tunnel were monitored. Finite element analysis (FEA), considering the small strain characteristics of the soft soil (Simpson 1992, Kung *et al.* 2007, Ardakani *et al.* 2014), was adopted to simulate this project. The simulation results were compared to the monitoring data, and the numerical simulation method was verified. On the basis of the case study, the tunnel deformations under different conditions were calculated systematically. The deformation characteristics of tunnels at different locations and under conditions with different deformation modes of retaining structures were compared and analyzed, and simultaneously, a method for the determination of the influence zones is discussed. In addition, two methods to predict tunnel deformation are proposed based on a large number of numerical simulations. One method is design charts, in terms of normalized tunnel deformation contours induced by adjacent excavations with different deformation modes and magnitudes, and the other is a design table for the determination of the influence zones of the excavation. Both methods were verified against practical engineering projects.

2. Case study and verification of the FEM simulation

2.1 Introduction of the case study

An excavation project in Tianjin, China to construct a three-level basement was located near an existing shield tunnel. The plan shape of the excavation was an irregular polygon. The main excavation depth was 15 m, and the partial excavation depths were 16.25 m and 17.55 m for the high-rise building towers. The environment surrounding the excavation was complicated. The excavation was surrounded by roads on its eastern, western, and northern sides. An existing tunnel was located on the southern side of the excavation, and the minimum distance was only 16.5 m. The plan layout of the excavation is shown in Fig. 2.

To control the deformation of the excavation and protect the tunnel, the following measurements were conducted. The excavation was divided into three parts, i.e., the southern, central, and northern excavations, as shown in Fig. 2. The southern excavation was excavated first, followed by the northern excavation. After the completion of the underground structure and the backfill of the southern and northern excavations, the central excavation began. The southern retaining structure of the southern excavation was a diaphragm wall with a thickness of 1200 mm, and the eastern and western sides were retained by diaphragm walls with a thickness of 1000 mm. The northern side was retained by contiguous piles ($\phi 900@1100$). Two levels of concrete struts were used. A row of isolation piles was constructed between the tunnel and the southern excavation to minimize the deformation of the tunnel. The monitored sections and points are illustrated in Fig. 2. The points DLQ 3, GLZ 3, and TCX 3 were the inclinometer monitoring points in the diaphragm wall, isolation pile, and soil, respectively.

2.2 Soil conditions

When the small-strain stiffness characteristic (i.e., the shear modulus of the soil is large and nonlinear at small strain conditions) is considered in the simulation of the excavation, the soil and tunnel deformations can be predicted more accurately (Simpson 1992, Kung *et al.* 2007). Therefore, the soil was modeled using the hardening soil model with small-strain stiffness, i.e., the HSS model in PLAXIS. The sub-soils at this site primarily consist of a sequence of alternating

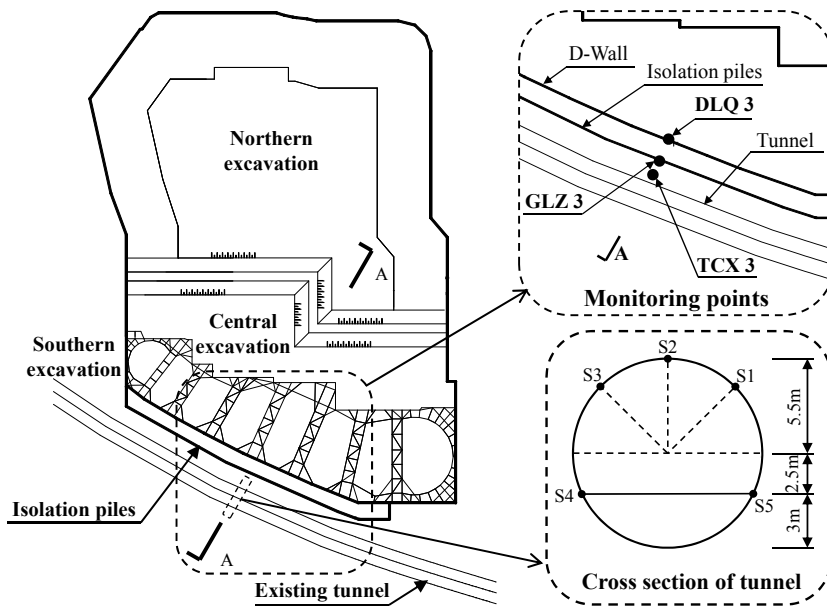


Fig. 2 Plan layout of the excavation

Table 2 Physical and mechanical parameters of the soils

Layer No.	Soil type	Thickness (m)	γ (kN/m ³)	c' (kPa)	ϕ' (°)	E_{50}^{ref} (MPa)	E_{oed}^{ref} (MPa)	E_{ur}^{ref} (MPa)	G_0^{ref} (MPa)	e
1-1	Miscellaneous fill soil	6.5	18.50	12.4	16.10	4.38	4.38	26.28	70.96	0.94
3-1	Silty clay	2.0	18.55	5.60	26.29	5.22	4.21	40.58	109.58	0.88
6-3	Silt	1.2	18.69	6.00	27.65	15.71	8.38	80.00	216.00	0.75
6-4	Silty clay	7.8	19.46	9.54	28.59	5.31	5.78	53.39	144.15	0.79
8-1	Silty clay	5.5	19.78	13.95	25.66	7.21	5.05	36.77	99.28	0.64
8-2	Silt	2.0	18.69	10.00	32.30	8.41	8.41	44.14	119.18	0.74
9-1	Silty clay	6.0	19.83	21.45	21.60	3.10	6.00	38.01	102.63	0.49
10-2	Silty sand	3.0	20.98	10.20	36.43	11.80	10.54	77.29	208.68	0.72
11	Silty clay	66.0	20.28	14.62	24.66	4.91	5.86	42.27	114.13	0.73

*Note: The value of $\gamma_{0.7}$ is set to 0.2×10^{-3} for all layers

silty clay and silt layers and partially consist of silty-fine sand layers. The distributions and parameters of the soil layers are listed in Table 2. The HSS model parameters were derived from laboratory tests using soil samples taken by a thin wall sampler.

2.3 FEM simulation of the excavation case

During the design period of this project, FEM simulations of the construction process of the excavation were conducted to evaluate its influence on the adjacent existing tunnel. A typical

section A-A (Fig. 1) was adopted for the analysis, as shown in Fig. 2.

The diaphragm wall, tunnel lining, contiguous pile, and isolation pile were modeled as linear elastic material with a Young's modulus of 30 GPa and a Poisson's ratio of 0.2. The contiguous piles were simulated by plate elements for simplicity, and the thickness of the plates was calculated based on the equivalent bending stiffness. The isolation piles were simulated by embedded pile elements in PLAXIS. The transverse effective rigidity ratio of the shield tunnel was set to 75% (Lee and Ge 2001) to include the influence of the segment joints on the rigidity of the tunnel.

The simulation procedure is listed below.

- (1) Generate the initial geostress.
- (2) Activate the plate elements of the diaphragm walls, contiguous piles and isolation piles.
- (3) Dewater to the bottom of the excavation.
- (4) In the southern excavation, excavate to a depth 3.6 m and construct the first level strut.
- (5) In the southern excavation, excavate to a depth of 8.4 m and construct the second level strut.
- (6) In the northern excavation, excavate to a depth of 9.6 m.
- (7) In the northern excavation, excavate to the bottom of the excavation.
- (8) In the southern excavation, excavate to the bottom of the excavation.

2.4 Comparison of the simulation results to the measured data

Fig. 4 shows the simulation results and measured data of the displacements of the diaphragm wall, isolation pile, and soil adjacent to the tunnel. Fig. 4 indicates that the simulation results are close to the measured data. The southern excavation deformed northward entirely when the northern excavation was conducted. Therefore, the maximum displacement of the diaphragm wall was 50 mm, which is relatively large.

Due to the unloading effect of the excavation, the tunnel deformed toward the excavation, as shown in Fig. 5. The deformation tendency of the tunnel calculated by the numerical simulation is the same as the measured data. However, the horizontal and vertical displacements of the simulation results are slightly larger than the measured data.

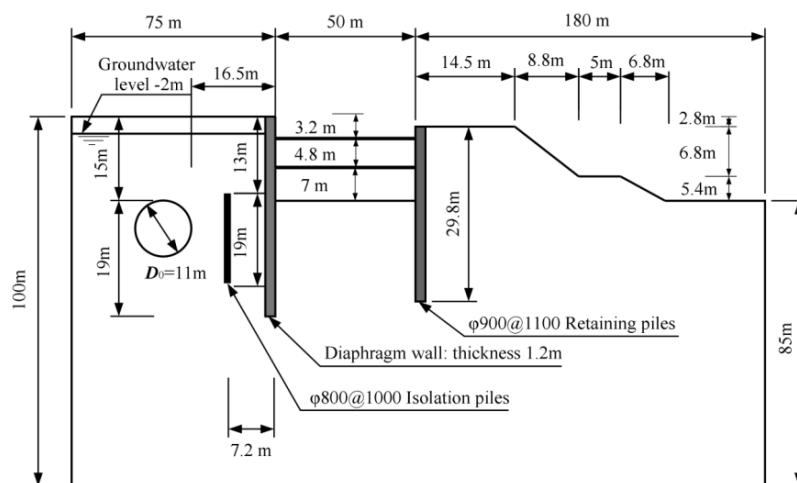


Fig. 3 Illustration of the section A-A of the excavation

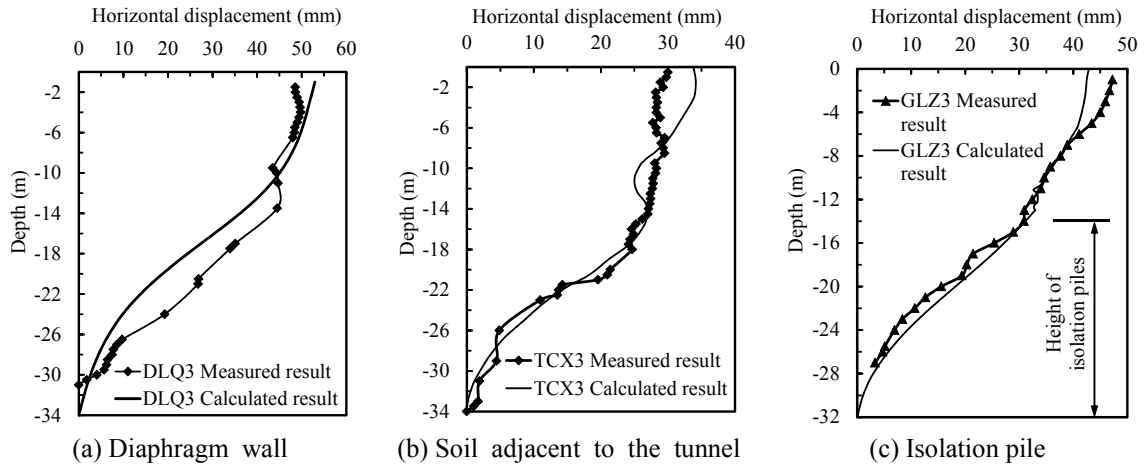


Fig. 4 Comparison between the calculated and measured horizontal displacements of DLQ3, TCX3, and GLZ3 at the end of excavation

In general, the capacity and feasibility of the FEM simulation using the HSS model is verified by the above comparison. The simulation method and similar soil parameters were used in the following sections of this paper to investigate the deformation characteristics of the adjacent tunnel and the influence zones of the excavation.

3. Finite element model for parametric studies

3.1 The geometry of the model

A series of simplified models were designed for the parametric study. One of the excavation depths was 18 m, which is a typical excavation depth for a two-floor metro station, as shown in Fig. 6. The embedded ratio of the diaphragm wall was 1. According to symmetry, half of the excavation was modeled. The width of the half excavation was 30 m. The width of the model

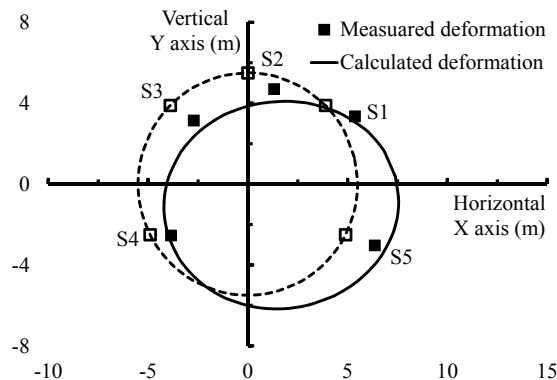


Fig. 5 Comparison between the calculated and measured deformation of the tunnel at the end of excavation (the tunnel deformation sketch is magnified 100 fold)

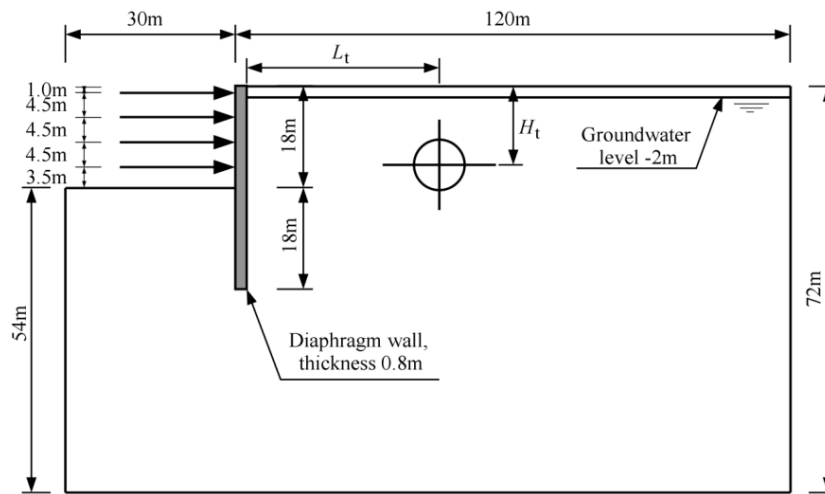


Fig. 6 Illustration of one of the excavation models in the parametric study

outside the excavation was 120 m. The relative location of the tunnel can be represented by two parameters, i.e., H_t and L_t , as shown in Fig. 6.

3.2 Soil parameters

The tunnel deformation characteristics are the primary concern of this study. In realistic soil conditions, there are several soil layers, and the tunnel may be located in any of them. The parameters of different soil layers will inevitably influence the tunnel deformation, which is not favorable for the study of deformation characteristics of tunnels in different locations. Consequently, a single typical soil layer (layer 8-1) was used in the model instead of realistic multi-layers. Soil layer 8-1 is a typical soil layer in the Tianjin area, and a large number of tunnels in Tianjin are located in this layer. The soil parameters of soil layer 8-1 are shown in Table 2.

3.3 Tunnel

The tunnel in this model was adopted based on the tunnel used in the Tianjin metro lines 2 and 3. The outer diameter of the tunnel was 6.2 m, and the thickness of the segments was 0.35 m. The transverse effective rigidity ratio of the tunnel was set to 75% (Lee and Ge 2001) to include the influence of the segment joints. The Young's modulus of the tunnel was set to 34.5 GPa (C50 concrete), and the Poisson's ratio was 0.2.

3.4 Working conditions

To systematically investigate the influence of the excavation on the tunnel deformation, several crucial factors were considered, such as the relative location of the tunnel (H_t and L_t), the deformation modes and maximum horizontal displacement (δ_{hmax}) of the retaining structure, and the excavation depth (H). The values of the above factors are listed in Table 3. In total, 1440 cases were calculated. For excavations with the same depth, different values of δ_{hmax} in Table 3 were achieved by the adjustment of the stiffness of the horizontal struts.

Table 3 Values of the influence factors considered in this study

Influence factor	Values of the influence factor	Number of values
L_t	6 m, 9 m, 12 m, 15 m, 21 m, 27 m, 33 m, 39 m	8
H_t	9 m, 18 m, 27 m, 36 m, 45 m	5
δ_{hmax}	0.167% H , 0.25% H , 0.333% H	3
Deformation modes	(a) the convex type; (b) the composite type; (c) the cantilever type; (d) the kick-in type	4
H	12 m, 15 m, 18 m	3

4. Deformation characteristics of tunnels for different deformation modes of the retaining structure

First, a typical excavation (excavation depth of 18 m with convex-type deformation of the retaining structure and a maximum displacement of 45 mm, i.e., 0.25% H) was adopted to analyze the deformation characteristics of adjacent tunnels at different locations. Then, the deformation characteristics under the conditions of different deformation modes of the retaining structure were analyzed and compared to that of the convex-type deformation mode.

4.1 Convex-type deformation mode of the retaining structure

4.1.1 Deformation characteristics of tunnels in different locations

The deformation and distortion of tunnels in different locations are illustrated in detail in Fig. 7. When the deformation type of the retaining structure was convex, the displacement of the top of the retaining structure was nearly zero, and the maximum displacement was located at the level of the excavation bottom. The deformation of the retaining structure caused tunnels in all locations to deform toward the excavation. However, as the burial depth and the distance between the tunnel and the excavation varied, the deformation characteristics of the tunnel also varied. According to the vertical displacements of the vault and the bottom of the tunnel, three zones can be recognized as listed below.

- Settlement zone: In the upper zone outside the excavation, the vault and bottom of the tunnel both settled. For tunnels located in this zone, especially very shallow tunnels, the vertical and horizontal displacements were both very severe and should therefore be carefully dealt with. As the burial depth increased, due to the convex-type deformation mode of the wall, the horizontal displacement of the tunnel increased, and the settlement decreased.
- Intermediate zone: In the zone below the settlement zone, the displacement of the vault of the tunnel was settlement, whereas the displacement of the bottom was upheaval. Therefore, this zone is called the intermediate zone. The vertical displacement of the tunnel center in this zone was relatively small. However, the horizontal displacement of the tunnel was significant and should be considered carefully.
- Upheaval zone: In the deeply seated zone, the displacements of the vault and bottom of the tunnel were upheaval-type displacements. However, the upheaval displacements were small compared to the vertical displacements in the settlement and intermediate zones.

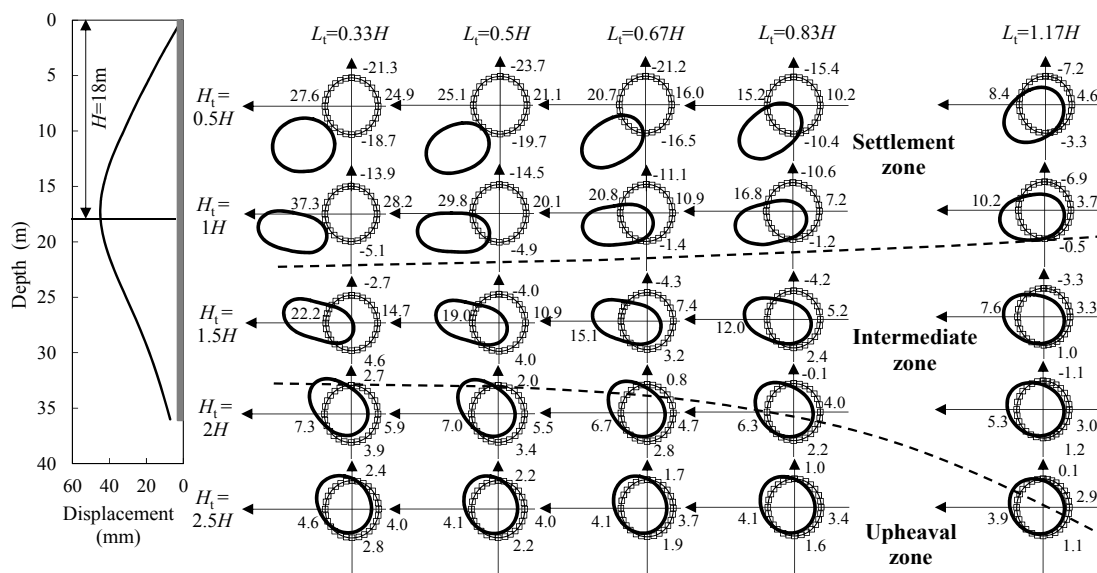


Fig. 7 The deformation of tunnels at different locations caused by convex-type deformation of the retaining structure (the tunnel deformation sketches are magnified 200 fold)

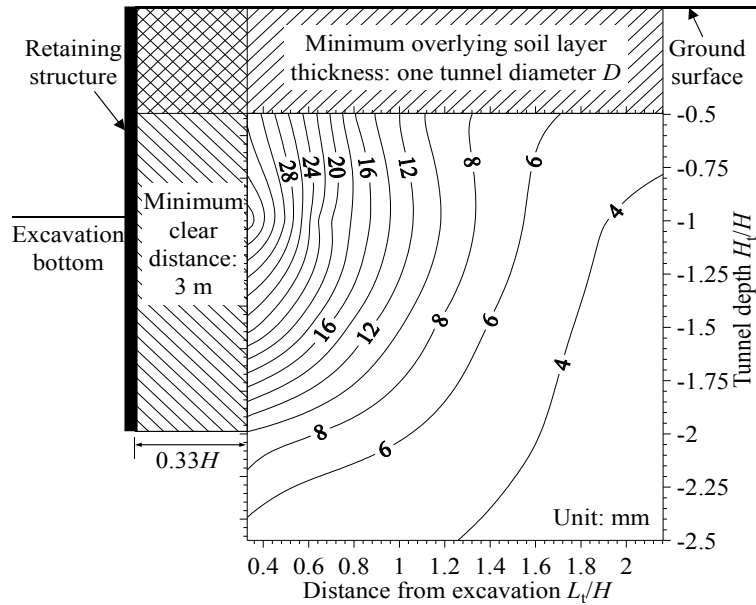
Based on above analysis, the deformation characteristics are different when the tunnel locations are different. In the settlement zone, the horizontal and vertical displacements were both large. However, in the intermediate zone, the horizontal displacement dominated. Therefore, protective measures for tunnels adjacent to excavations should be proposed considering the location of the tunnels.

Based on the results in Fig. 7, the contours of the maximum horizontal and vertical displacements of a tunnel in different locations can be depicted as in Fig. 8. The tunnel cannot be in a zone very close to the excavation (3 m outside the excavation; No. 854 of Shanghai Municipal Statute 1994) or in the zone near the ground surface (at a depth less than the tunnel diameter; Code for Design of metro GB50157-2003). Therefore, the contours were not included in these zones. As seen in Fig. 8, when the deformation mode of the retaining structure was convex-type, the horizontal displacement of the tunnel located near the excavation bottom was largest. The settlement of the tunnel became smaller as the burial depth of the tunnel became larger, and gradually, the maximum vertical displacement resulted in upheaval. However, the maximum upheaval was only 5 mm, indicating that the tunnel was not affected significantly by the rebound effect of the excavation.

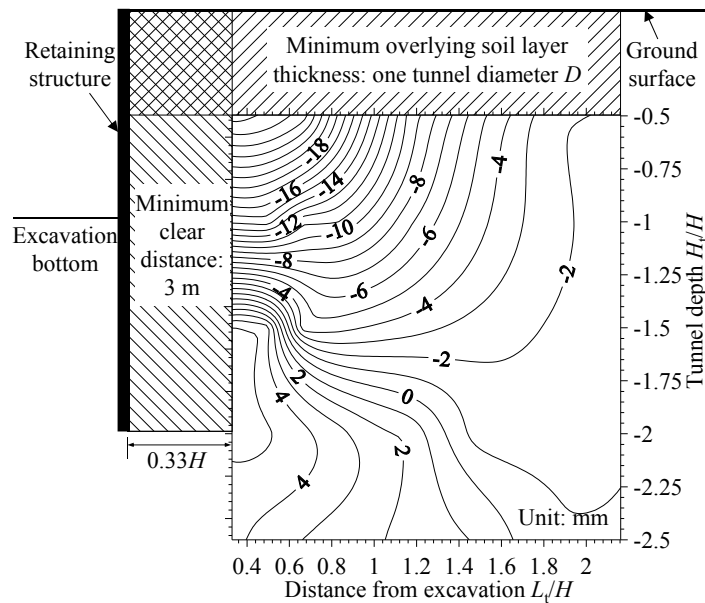
In addition, Fig. 8 can be used as a design chart for the estimation of the horizontal and vertical displacements of tunnels located in different positions with respect to the excavation with a convex deformation mode and a maximum retaining structure displacement of 45 mm.

4.1.2 Influence zones

The aforementioned standards (No. 854 of Shanghai Municipal Statute 1994, GJJ/T 202-2013, GB 50911-2013) proposed several deformation control criteria for tunnels. Based on these standards, three deformation control values, i.e., 5 mm, 10 mm, and 20 mm, were adopted for the partitions of the influence zones of the excavation on the tunnels. Fig. 9(a) shows the contours of



(a) The maximum horizontal displacement

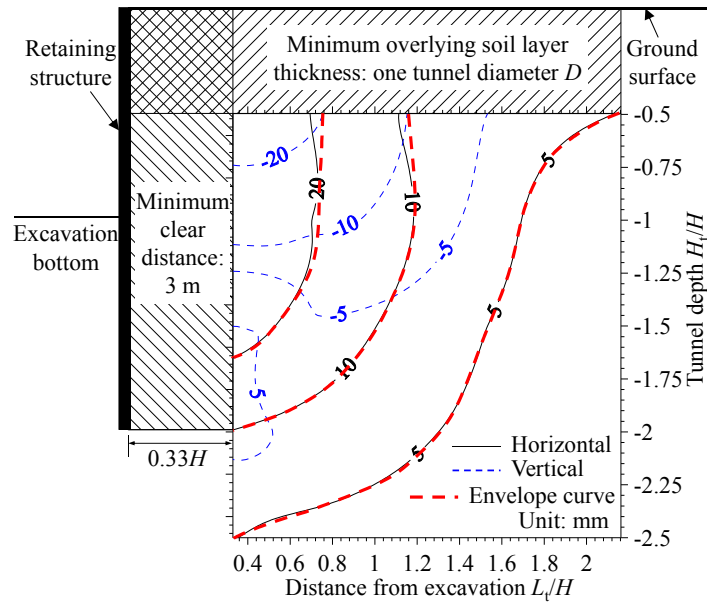


(b) The maximum vertical displacement

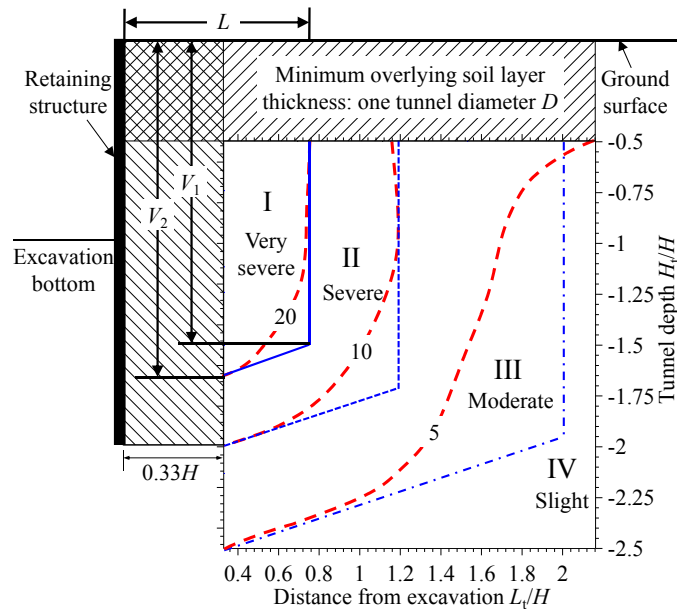
Fig. 8 The maximum displacement contours of tunnels caused by convex-type deformation of the retaining structure (derived from the results of 40 FEM models with tunnels in different positions)

the deformation control values. The envelope curves (dashed red lines), which comprise the ranges of both the horizontal and vertical contours of a control value, are drawn in Fig. 9(a). In general, the contour of the horizontal displacement is much larger than that of the vertical displacement;

therefore, the envelope curves were primarily determined by the contours of the horizontal displacement besides the parts in the shallow soil layer. When the center of the tunnel is located inside the envelope curve of a control value, in most cases, the displacement of the tunnel in at



(a) Envelope curves



(b) Influence zones

Fig. 9 Envelope curves of different deformation control criteria and influence zones for the convex-type deformation of the retaining structure

least one direction (horizontal or vertical) will exceed the control value.

As shown in Fig. 9, as the deformation control value decreases (i.e., the deformation control becomes strict), the envelope curve enlarges. This indicates that the deformation cannot satisfy the strict control criterion when the tunnel is close to the excavation. If the influence zones of an excavation are known, whether the deformation of the existing tunnel can satisfy the deformation control criterion can be predicted according to the relative location of the tunnel.

The irregular envelope curves in Fig. 9(a) are not convenient for applications in practical engineering. Therefore, the envelope curves have been simplified to polylines to serve as boundaries of the different influence zones. As shown in Fig. 9(b), three polylines represent the control values of 20 mm, 10 mm, and 5 mm, respectively. The four influence zones divided by these polylines can be called the very severe influence zone, the severe influence zone, the moderate influence zone, and the slight influence zone, respectively.

Each influence zone curve can be represented by three parameters: L , V_1 , and V_2 . L is the horizontal distance of the polyline boundary to the excavation, V_1 is the distance of the turning point of the polyline to the ground surface, and V_2 is the vertical distance of the polyline boundary to the ground surface. The parameters (L , V_1 , and V_2) of the very severe influence zone are shown in Fig. 9(b) as an example.

4.2 Composite-type deformation mode of the retaining structure

4.2.1 Deformation characteristics of the tunnels in different locations

Fig. 10 shows the deformations of tunnels in different positions under the composite-type deformation mode of the retaining structure. The deformation characteristics of tunnels for the composite-type deformation mode are similar to that for the convex-type deformation mode. The partition of the settlement zone, intermediate zone, and upheaval zone are also nearly the same as that of the convex-type deformation mode. However, because the horizontal displacement of the

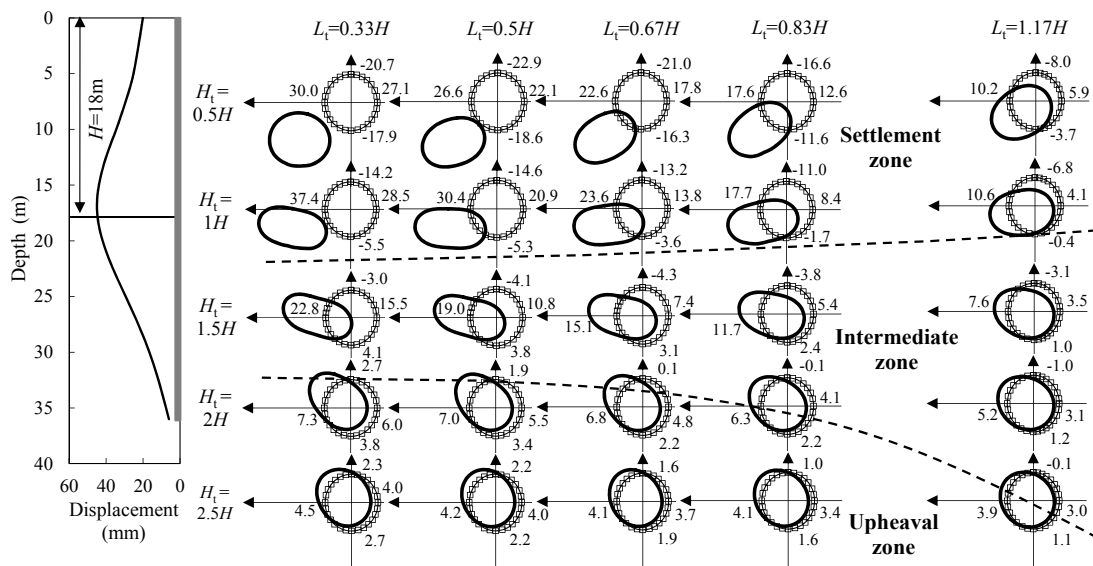


Fig. 10 The deformation of tunnels at different locations caused by composite-type deformation of the retaining structure (the tunnel deformation sketches are magnified 200 fold)

top of the retaining structure with composite-type deformation was larger than that with the convex-type mode, the horizontal displacements of the shallow tunnels, e.g., the tunnels with a burial depth of $0.5H$, were slightly larger.

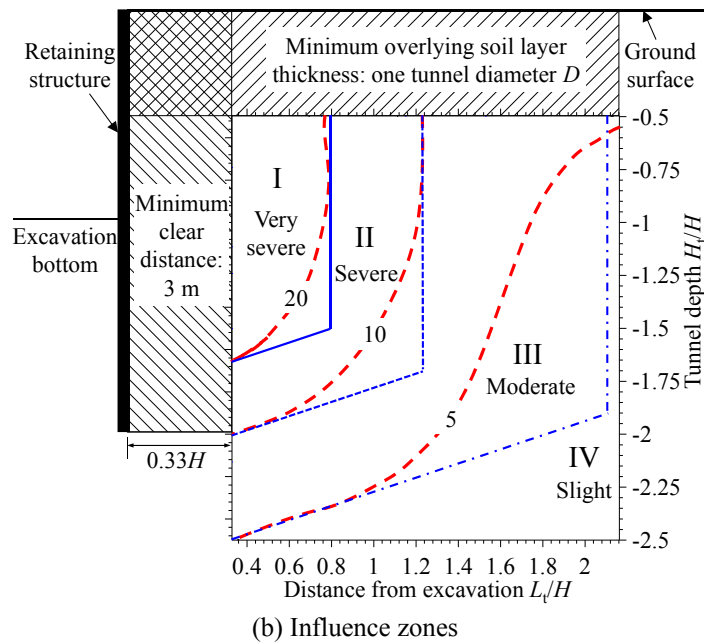
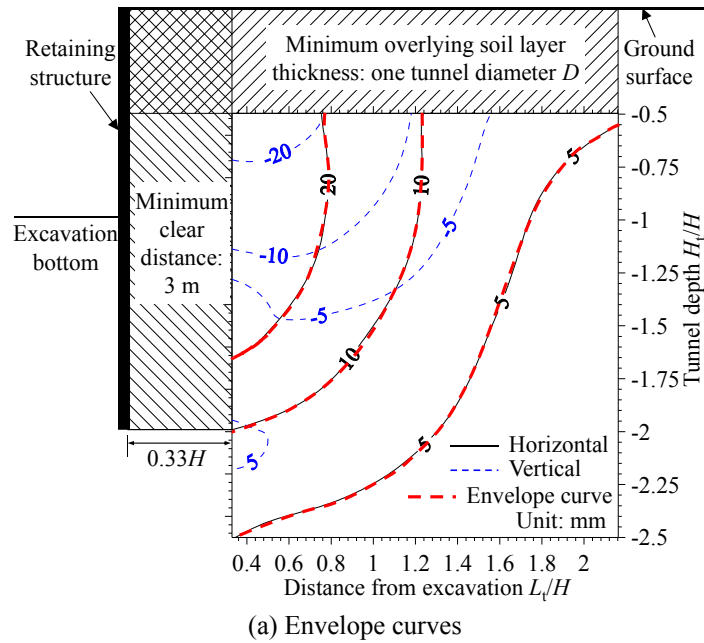


Fig. 11 Envelope curves of different deformation control criteria and influence zones for the composite-type deformation of the retaining structure

4.2.2 Influence zones

Fig. 11 shows the displacement contours and influence zones for the composite-type deformation mode. In Fig. 9, for the convex-type mode, the envelope curves of the deformation control values (20 mm and 10 mm) in the shallow soil layer were determined by the vertical displacement contours. However, for the composite-type case, because the horizontal displacements in the shallow soil layer were slightly larger than the vertical displacements, the three envelope curves were determined entirely by the horizontal displacement contours, as shown in Fig. 11(a). The shapes and sizes of the influence zones for the composite-type deformation mode are similar to those for the convex-type mode, as shown in Fig. 11(b). However, the sizes of the influence zones in the horizontal direction are slightly larger.

4.3 Cantilever-type deformation mode of the retaining structure

4.3.1 Deformation characteristics of the tunnels in different locations

Fig. 12 shows the deformations of tunnels in different positions under the cantilever-type deformation mode of the retaining structure. Compared to the convex-type deformation mode, the maximum horizontal displacement of the retaining structure was at the top rather than at the excavation bottom. Even though the maximum displacements of the retaining structures are the same, the horizontal and vertical displacements (especially the vertical displacement) of the tunnel in the cantilever-type mode condition are smaller than that of the tunnel at the same location in the convex-type mode condition. In addition, compared to the convex-type deformation mode condition, the settlement zone is much smaller, and the intermediate zone is larger in the cantilever-type mode condition.

4.3.2 Influence zones

As shown in Fig. 13, because the vertical displacements of the tunnels in different positions

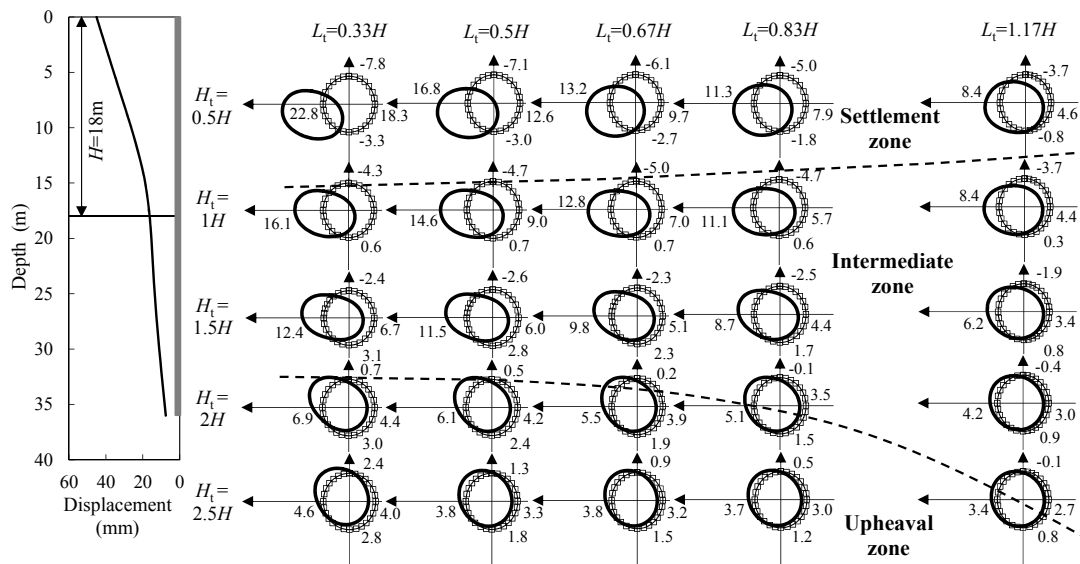
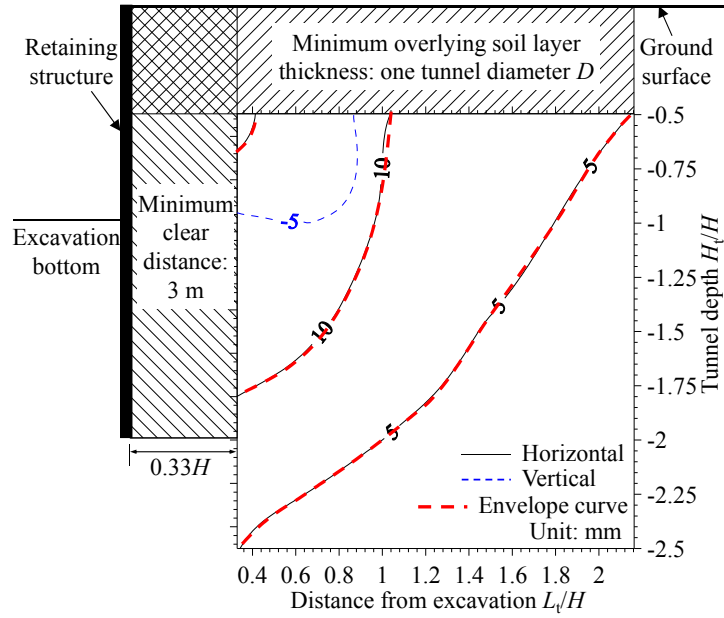
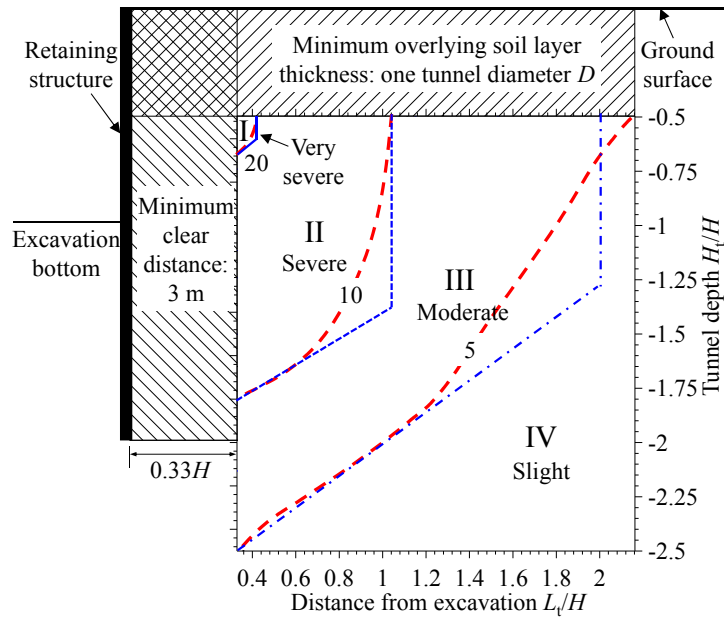


Fig. 12 The deformation of tunnels at different locations caused by cantilever-type deformation of the retaining structure (the tunnel deformation sketches are magnified 200 fold)



(a) Envelope curves



(b) Influence zones

Fig. 13 Envelope curves of different deformation control criteria and influence zones for cantilever-type deformation of the retaining structure

were relatively small, the envelope curves of the deformation control values were mainly determined by the horizontal displacement contours. Compared to the convex-type mode condition,

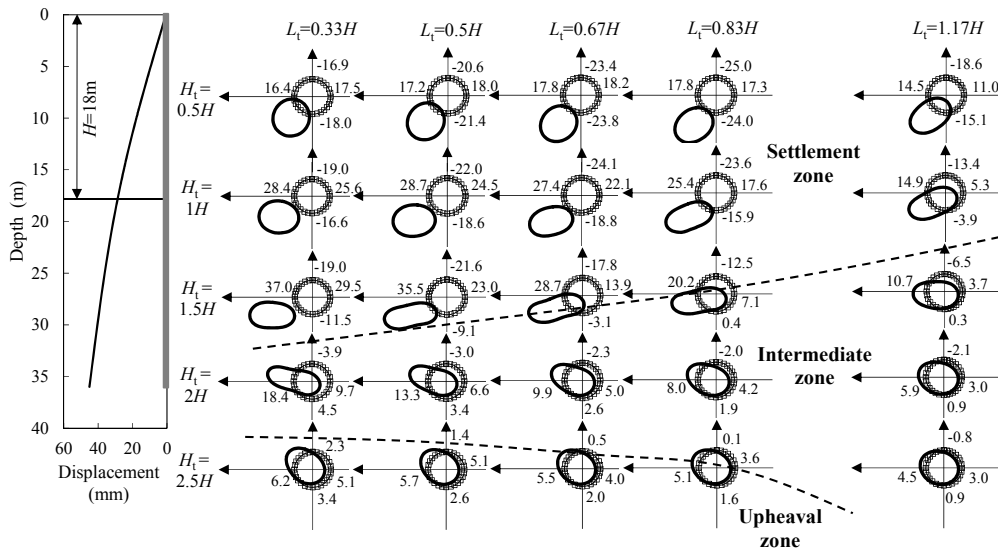


Fig. 14 The deformation of tunnels at different locations caused by kick-in-type deformation of the retaining structure (the tunnel deformation sketches are magnified 200 fold)

the sizes of the influence zones (especially the very severe influence zone) in the cantilever-type mode condition are much smaller both in the horizontal and in the vertical directions.

4.4 Kick-in-type deformation mode of the retaining structure

4.4.1 Deformation characteristics of the tunnels in different locations

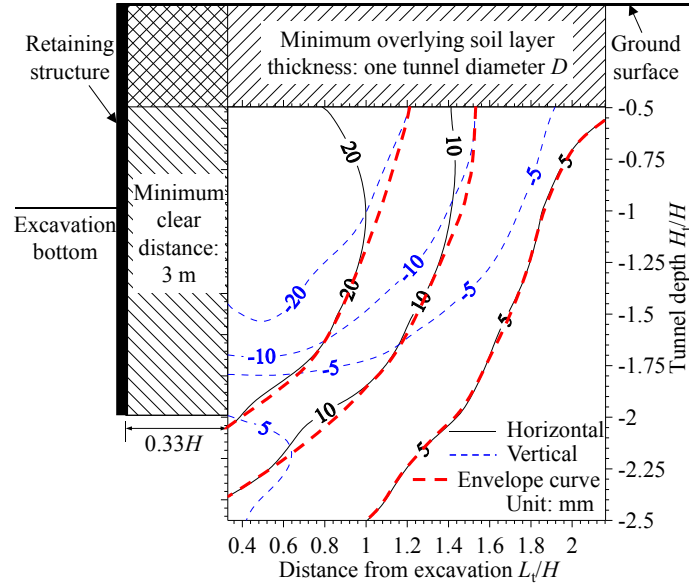
Fig. 14 shows the deformations of tunnels in different positions under the kick-in-type deformation mode of the retaining structure. Because the maximum displacement of the retaining structure was at the bottom of the retaining structure, the settlement zone was much larger and deeper than in the convex-type mode condition. Correspondingly, the intermediate and upheaval zones moved downward compared to the convex-type mode condition. In addition, the convergence deformations of the tunnels are more severe than those of the convex-type mode, especially for tunnels near the bottom of the retaining structure. In general, when the deformation mode of the retaining structure is kick-in type, the deformations of the adjacent tunnels are very severe. Therefore, the kick-in type deformation mode of the retaining structure should be avoided in practical engineering.

4.4.2 Influence zones

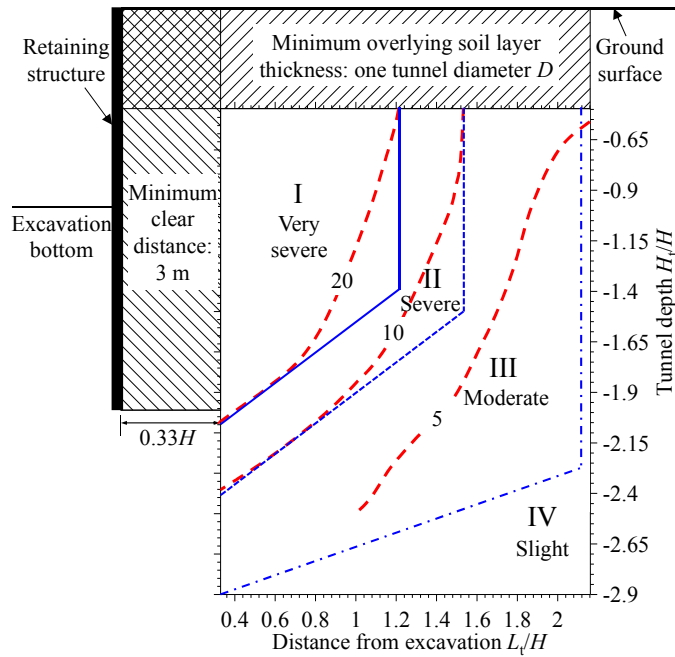
As shown in Fig. 15, the envelope curves of the deformation control values in the shallow soil layer were determined by the vertical displacement contours, whereas the envelope curves in the deep soil layer (such as the soil layer near the bottom of the retaining structure) were determined by the horizontal displacement contours. The sizes of the influence zones of the kick-in-type mode condition were much larger than that of the convex-type mode condition in both the horizontal and the vertical directions.

4.5 Comparison of the influence zones under different deformation mode conditions

The geometry parameters of the influence zones in Sections 4.1-4.4 are summarized in Table 4.



(a) Envelope curves



(b) Influence zones

Fig. 15 Envelope curves of different deformation control criteria and influence zones for kick-in-type deformation of the retaining structure

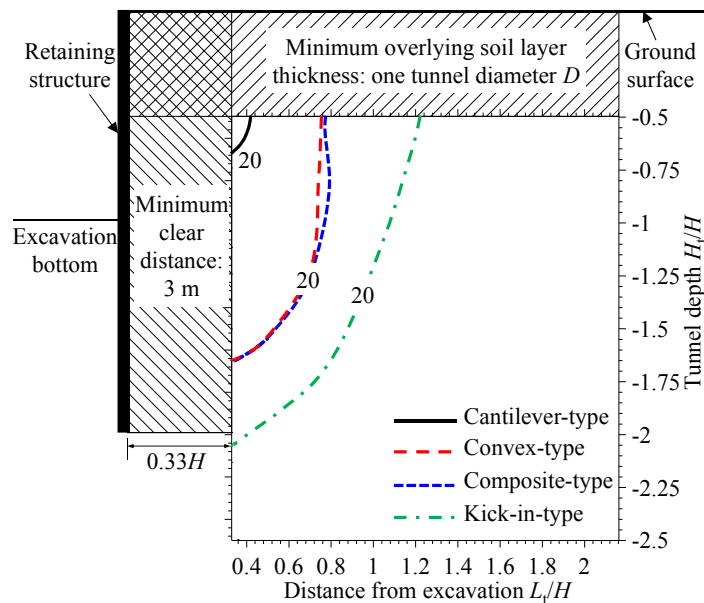
Table 4 can be used as a design table to determine the influence zone in which the existing tunnel is located in under certain conditions (e.g., excavation depth: 18 m, displacement of retaining

structure: 45 mm). Figs. 16 and 17 show a comparison of the envelope curves of the deformation control values and the geometry parameters of the influence zones for different deformation modes, respectively. It can be seen in Figs. 16 and 17 that when the maximum displacements of the retaining structures are the same, the influence zones are significantly different for the different deformation modes of the retaining structure. The influence zones are smallest under the condition of the cantilever-type deformation mode and largest under the condition of the kick-in-type deformation mode. The influence zones of the composite-type mode are close to and slightly larger than that of the convex-type mode.

Based on the above analysis, when an excavation is adjacent to an existing tunnel, besides the restriction of the maximum displacement of the retaining structure, it is also necessary to control the deformation mode of the retaining structure according to the position of the tunnel. If the maximum displacement of the retaining structure can be controlled, a retaining system with a cantilever-type deformation mode is the best option to protect the tunnel. The second best option is

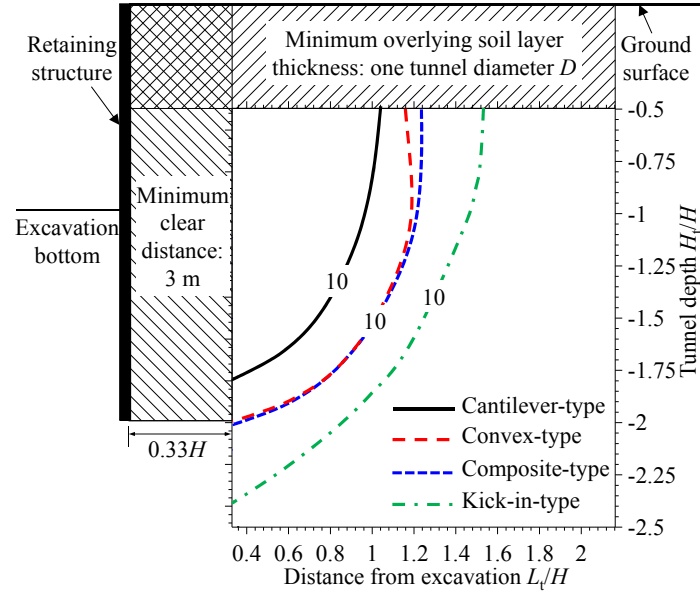
Table 4 Design table of the influence zones (excavation depth: 18 m, displacement of retaining structure: 45 mm) derived from the results of 160 FEM models

Deformation mode	Control value: 20 mm			Control value: 10 mm			Control value: 5 mm		
	L	V_1	V_2	L	V_1	V_2	L	V_1	V_2
Convex-type	0.75	1.50	1.65	1.20	1.71	2.00	2.00	1.95	2.50
Composite-type	0.80	1.50	1.66	1.23	1.70	2.00	2.10	1.90	2.50
Cantilever-type	0.42	0.60	0.67	1.04	1.38	1.82	2.00	1.38	2.50
Kick-in-type	1.22	1.39	2.05	1.54	1.50	2.41	2.12	2.27	2.90

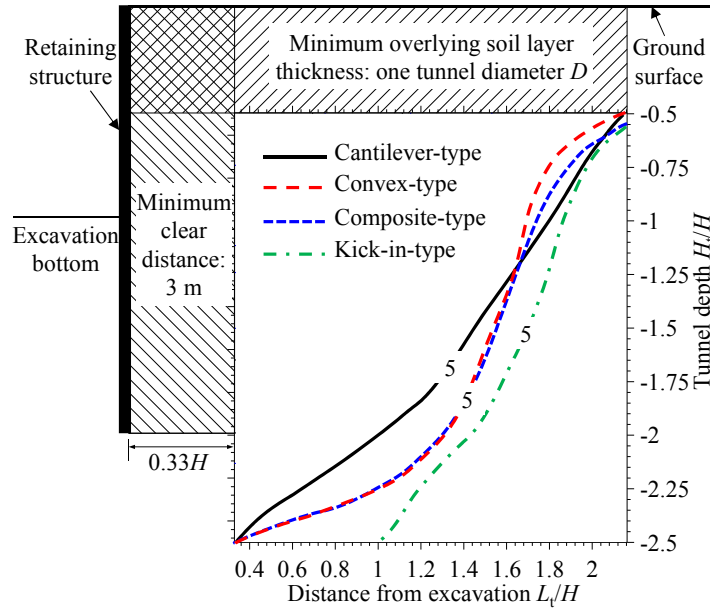


(a) Control value of 20 mm

Fig. 16 Comparison of the influence zones under different deformation modes of the retaining structure



(b) Control value of 10 mm



(c) Control value of 5 mm

Fig. 16 Continued

the convex-type mode or the composite-type mode. However, when the tunnel is located near the bottom of the excavation, the deformation of the tunnel should be carefully monitored under the convex-type and composite-type deformations. To prevent extreme deformation of the adjacent tunnel, the kick-in-type deformation mode of the retaining structure should be avoided. For deep

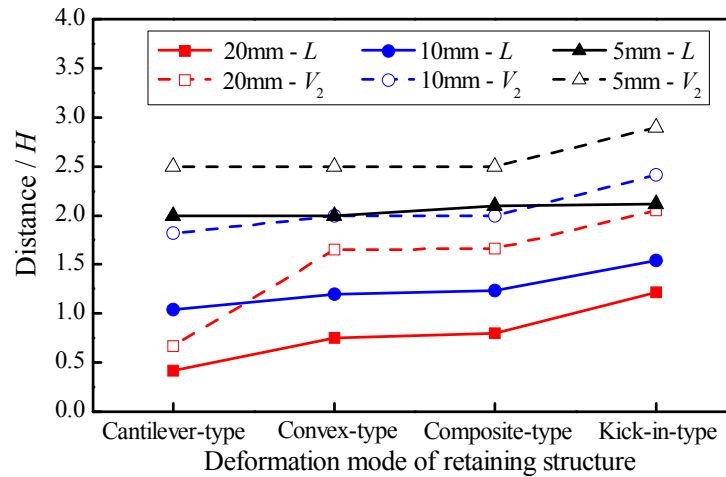


Fig. 17 Comparison of the geometry parameters of the influence zones under different deformation modes

buried tunnels near the bottom of the retaining structure, the influence on the tunnel of an excavation with the kick-in-type deformation mode is especially serious.

5. Prediction methods to estimate tunnel deformation induced by adjacent excavation

In Section 4, two methods to evaluate the influence of the excavation on the adjacent tunnel were proposed. The first method is to use a design chart (e.g., Fig. 8) for quantitative predictions of the tunnel displacements. The second method is to determine which influence zone (very severe, severe, moderate, or slight) the tunnel is located in from a design table, such as Table 4, to determine the influence degree of the excavation on the tunnel. However, these two methods in Section 4 can only be applied under specific conditions. Therefore, they will be optimized and enriched in this section.

5.1 Design charts for the estimation of tunnel deformation

5.1.1 Dimensional analysis

The design chart in Fig. 8 and the design table of influence zones proposed in Section 4 can be applied only to an excavation with a depth of 18 m. In addition, a design table or design chart in terms of dimensional parameters is not very convenient in practical engineering. It is better to use non-dimensional or normalized parameters. In deep excavation engineering, the excavation depth H is a key parameter that can significantly influence the deformation behavior of the ground and the adjacent tunnel. Here, the excavation depth H is adopted to normalize the deformation of the retaining structure and adjacent tunnel.

To examine whether the normalized deformation of the adjacent tunnel induced by the normalized deformation of the retaining structure is independent of the excavation depth H , the influences of excavations with different depths and different retaining structure deformations were calculated and compared. Three typical excavation depths H , i.e., 12 m, 15 m, and 18 m, and three typical normalized deformations of the retaining structure δ_{hmax} , i.e., $0.167\%H$, $0.25\%H$, and

0.333% H , were considered.

Based on the results in Section 4, the influence zone is primarily dominated by the horizontal displacement contour of the tunnel. Therefore, the contours of the normalized horizontal displacement of the tunnel induced by excavations with different excavation depths and the same normalized retaining structure displacement (0.25% H) were compared, as shown in Fig. 18. Because the result of the convex-type is similar to that of the composite-type, to make the paper more concise, it is not given in Fig. 18. For different excavation depths, the contours of the normalized horizontal displacement of the tunnel are nearly identical and close to each other. Therefore, the representation of the contours for different excavation depths by a unified contour, i.e., the red contour in Fig. 18 (the contour of the average result of those three depths), is reasonable. For the other two normalized deformations of the retaining structure δ_{hmax} , i.e., 0.167% H and 0.333% H , the results show the same conclusion.

5.1.2 Design charts

As listed in Table 3, 1440 cases were calculated. Based on the results, the design charts for the estimation of tunnel deformation (maximum horizontal and vertical displacements) induced by adjacent excavations were proposed, as shown in Appendix A: Figs. A1-A12. These design charts are presented in the form of contours on a grid of L_i/H ratios on the x-axis and H_i/H ratios on the y-axis. Non-dimensional or normalized versions of the parameters are used in the design charts. Therefore, the displacements of tunnels located at varying positions relative to excavations with different depths, different deformation modes, and different deformation magnitudes can be estimated before the construction of the excavation following the guidelines below.

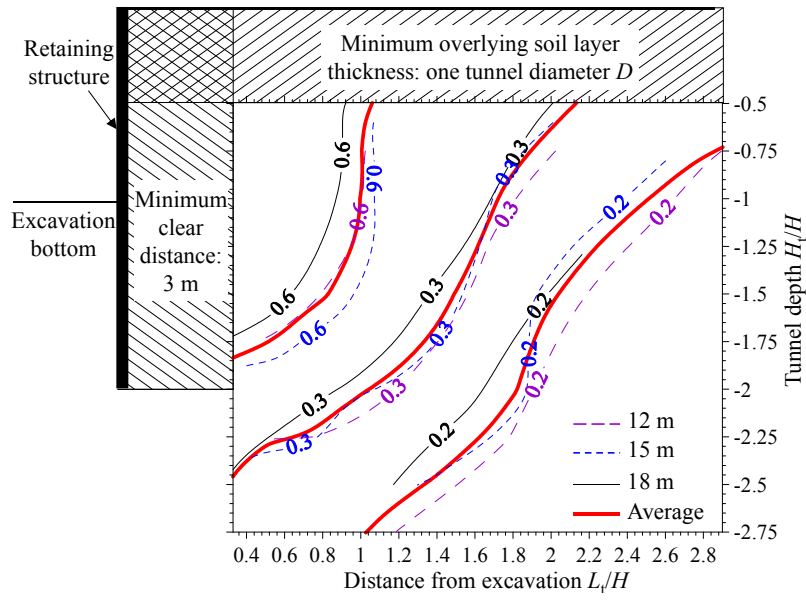
- (a) Determine the deformation mode and maximum horizontal displacement δ_{hmax} of the retaining structure according to the calculated or predicted results in the design period of the excavation.
- (b) Calculate the L_i/H ratio, H_i/H ratio and δ_{hmax}/H ratio. Choose a closest δ/H value of the δ_{hmax}/H ratio from the values of 0.167% H , 0.25% H , and 0.333% H . Based on the deformation mode and the δ/H value, the design charts for this excavation can be determined. Note that if δ/H is smaller than the δ_{hmax}/H ratio, the displacements estimated from the design charts might be smaller than the precise values, which are on the risky side.
- (c) Obtain the normalized values of the horizontal and vertical displacements of the tunnel from the corresponding design charts.
- (d) Convert the normalized values obtained in Step (c) into dimensional values using the excavation depth H .

These design charts were derived from FEM results based on simplified ground conditions and idealized geometric configurations. The simplified ground condition was based on the soft soil condition in Tianjin, and the tunnel used in the simulation was a circular tunnel with a diameter of 6.2 m and a precast concrete segment lining. Therefore, the design charts should be applied to engineering projects with similar conditions. In addition, the prediction results derived from these design charts are highly approximate and should be taken as a reference in the decision making process. To obtain more precise and detailed results, a site-specific analysis should be conducted.

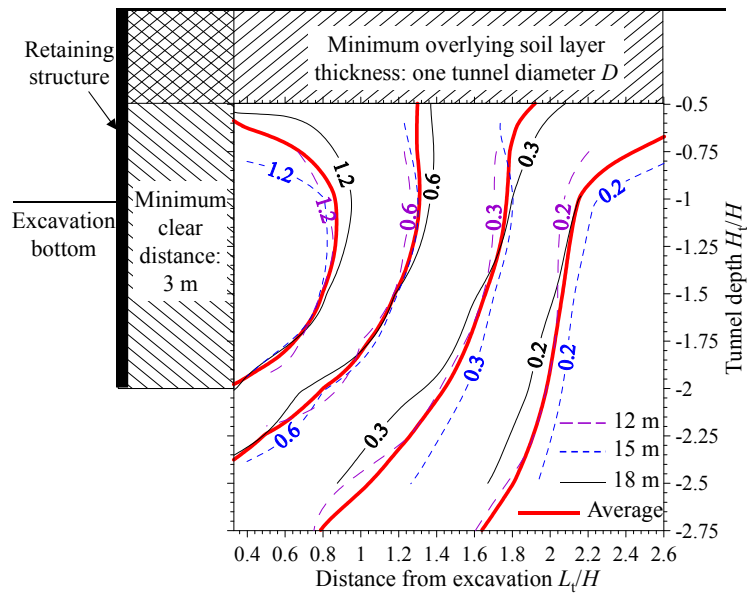
5.2 Design table for the determination of the influence zones

The design charts in Section 5.1 provide an approach for the quantitative estimation of the

tunnel deformation. Another method to directly observe the influence degree of the excavation on the tunnel is to sketch the influence zones of the excavation. To determine the influence zones for the tunnel conveniently and quickly, the geometric parameters of the influence zones under 36 conditions are summarized in Appendix B based on the FEM results. According to the influence



(a) Cantilever-type (unit: ‰H)



(b) Kick-in-type (unit: ‰H)

Fig. 18 A comparison of normalized horizontal displacement contours of tunnels induced by excavations with different depths

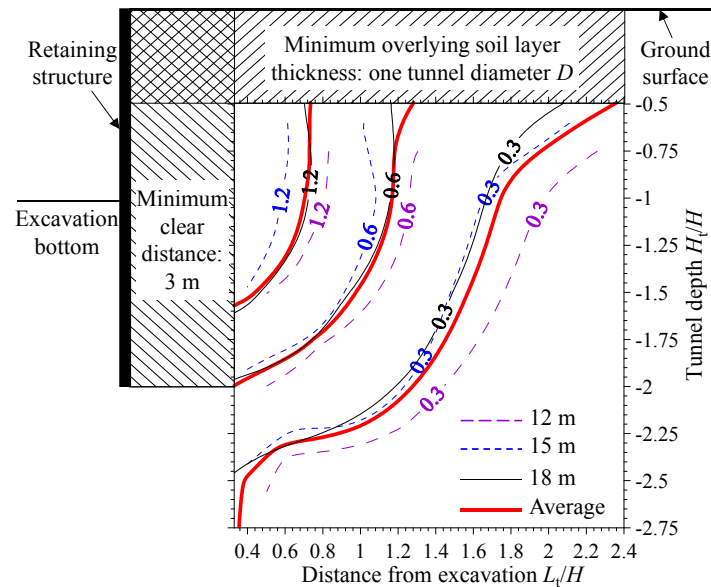
(c) Composite-type (unit: ‰ H)

Fig. 18 Continued

zones derived from Table B1 and the relative position of the tunnel, the influence zone where the tunnel is located can be clearly observed.

6. Analysis of engineering projects using the design charts and design table

Most of the excavation cases in Table 1 were in coastal soft-soil areas and had soil conditions that were similar to the soft soil conditions in Tianjin. In addition, the existing tunnels in those cases were primarily shield tunnels. Therefore, some cases with enough information (Cases 1, 2, 3, 10, 18, 22, and 25) in Table 1 were adopted for the illustration and verification of the application of the design charts and design table proposed in Section 5.

6.1 Application of the design charts

The retaining structures in Cases 1, 2, 3, 10, 18, 22, and 25 all exhibited composite-type deformation. Therefore, they were analyzed using the design charts for the composite-type deformation. Following the guidelines in Section 5.1.2, the predicted displacements of the tunnels in these cases can be derived. A comparison of the measured data and the predicted data using the design charts are shown in Table 5. It can be seen from Table 5 that most predicted results are close to but slightly larger than the measured results. This is because the predicted displacements present the largest displacements of the ring of the tunnel. However, the measured displacements represent the displacements of certain points on the ring of the tunnel. Therefore, it is reasonable for the predicted results to be larger than the measured results. The influence zones in which the tunnels are located can be determined according to the predicted displacements, as shown in Table 5. The predicted influence zones were mostly consistent with the actual situations of the projects,

Table 5 Comparison of the measured data and the predicted data using the design charts

Case No.	δ_{hmax}	Measured data		Predicted data		Influenced zone
		Horizontal displacement	Vertical displacement	Horizontal displacement	Vertical displacement	
1	0.252% <i>H</i>	27	-33	36.52	-20.95	I
2	0.114% <i>H</i>	9	-5	14.34	-8.06	II
3	0.453% <i>H</i>	50		23.68	-10.83	I
10-1	0.146% <i>H</i>		2.85	10.23	-7.84	II
10-2	0.146% <i>H</i>		-2.4	3.41	-1.40	IV
18	0.043% <i>H</i>		-5	10.71	-7.88	II
22	0.150% <i>H</i>	1.52	-4.11	9.22	-7.19	III
25	0.284% <i>H</i>	8.89	-5.9	11.71	-7.10	II

such as in Cases 1 and 3, where the tunnels were damaged and were obviously in very severe influence zones.

In Case 3, the maximum horizontal displacement measured by the inclinometers was 54 mm, which was close to 0.333%*H*. The predicted results were derived using the design charts for 0.333%*H*. However, according to the numerical simulation results, the toe of the inclinometer moved by 10 mm, and the actual maximum horizontal displacement should be approximately 72 mm (Hwang *et al.* 2011). Therefore, the predicted results in Table 5 underestimated the displacements of the tunnel in Case 3.

6.2 Application of the design table to determine the influence zones

According to the horizontal displacement of the retaining structure δ_{max} and the excavation depth *H*, the influence zones of the excavation in each case can be determined from Table B1, as shown in Fig. 19. The predicted results of the influence zones generally reflect the actual situations of the projects. It can be seen that the tunnels in Cases 1 and 3 were located in the very severe influence zone. However, there were no special measures taken in Cases 1 and 3 to protect the tunnel. Consequently, the tunnel in Case 1 deformed severely and, as a result, the invert slab became detached from the lining segments and had to be replaced (Hwang *et al.* 2011). In Case 3, the convergence deformation of some rings exceeded the Action Level, and internal bracings were installed in the tunnel to limit the deformation (Hwang *et al.* 2011). The tunnels in Cases 2 and 10 were in the severe influence zone, and certain protective measures were applied in these cases to reduce the tunnel deformation. In Case 2, cement-soil mixed piles were constructed around the tunnel. In Case 10, a zoned construction method with a temporary diaphragm wall was used. In addition, the influence zones determined using the design table were consistent with those determined in Section 6.1; however, the sketches in Fig. 19 offer an opportunity to directly observe the influence degree of the excavation on the tunnel.

A large number of FEM simulations considering the small-strain characteristics of soil were conducted to investigate the influence of excavation on adjacent tunnels. The deformation characteristics of tunnels in different positions relative to the excavation were analyzed.

Simultaneously, the differences in tunnel deformation characteristics under different deformation modes of the retaining structure were analyzed and discussed. Furthermore, two

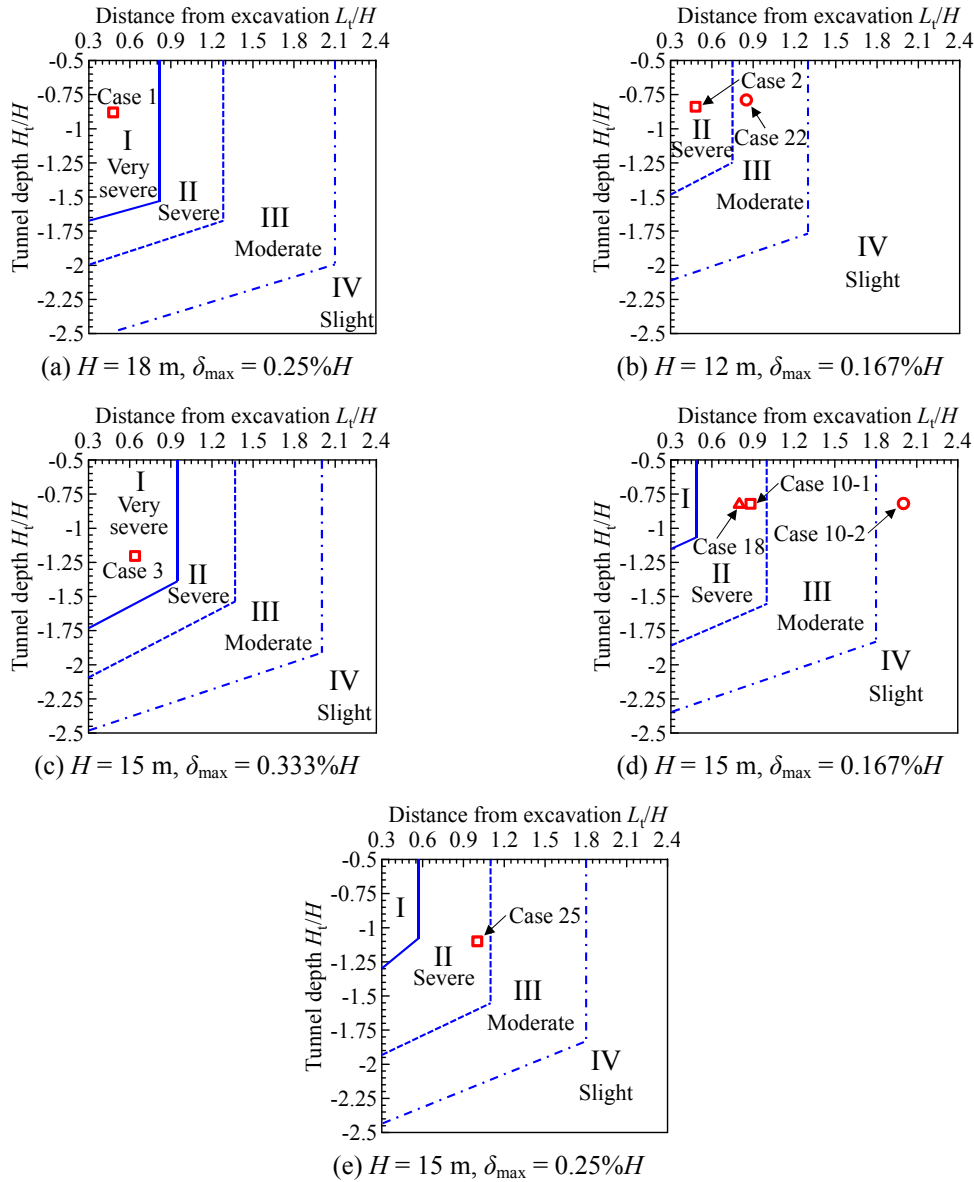


Fig. 19 The influence zones for some cases in Table 1

methods to predict the influence of the excavation on an adjacent tunnel were proposed. The main conclusions can be summarized as below.

- Tunnels next to an excavation move toward the excavation in the horizontal direction. According to the vertical displacements of the tunnel vault and bottom, there are three zones, i.e., the settlement zone, the intermediate zone, and the upheaval zone, that can be recognized outside the excavation from the ground surface to the deep-seated soil layer.
- According to the influence degree of the excavation on the tunnel, i.e., the magnitude of the tunnel deformation induced by the excavation, the area surrounding the excavation can be

separated into four influence zones: a very severe influence zone, a severe influence zone, a moderate influence zone, and a slight influence zone. The partition of the influence zones is based on the displacement contours of the deformation control values, which are determined based on the values suggested in several standards in China.

- The deformation mode of the retaining structure has a significant influence on the deformation of a tunnel even when the deformation magnitudes of the retaining structure are the same. Therefore, to protect the tunnel adjacent to the excavation, in addition to the restriction of the maximum displacement of the retaining structure, it is also necessary to control the deformation mode of the retaining structure according to the position of the tunnel. When the maximum displacements of the retaining structures are the same, the influence zones are smallest for the cantilever-type deformation mode and largest for the kick-in-type deformation mode. The influence zones of the composite-type mode are close to and slightly larger than those of the convex-type mode. Because the deformations of the adjacent tunnels are very severe, the kick-in type deformation mode of the retaining structure should be avoided in practical engineering.
- The contours of the normalized tunnel displacements (normalized by excavation depth) of tunnels in different positions were found to be nearly independent of the excavation depth. Therefore, design charts in the form of normalized displacement contours independent of the excavation depth were given based on the substantial FEM simulation results. These design charts can be used for a quantitative estimation of the displacements of tunnels located in different positions relative to excavations with different depths, different deformation modes, and different deformation magnitudes.
- A method proposed to directly observe the influence degree of the excavation on the tunnel is to sketch the influence zones of the excavation and to determine which influence zone the existing tunnel is located in. The geometric parameters of the influence zones under various conditions are summarized and given in a design table.
- The accuracy and applicability of the above two methods were verified with practical engineering projects. However, the design charts and design table were derived from the FEM results based on simplified ground conditions and idealized geometric configurations. Therefore, they should be applied to engineering projects with similar conditions to those used in this study. Note that the prediction results derived from the design charts and table are highly approximate and should be taken as a reference in the decision making process. In addition, similar design charts and design tables can be derived based on other specific local conditions for local usage.

Acknowledgments

This work was supported by the Key Projects in the National Science & Technology Pillar Program during the Twelfth Five-year Plan Period (Grant No. 2012BAJ01B02-03), the China Postdoctoral Science Foundation (Grant No. 2014M561186), and the National Natural Science Foundation of China (Grant No. 51508382). Their support is gratefully acknowledged.

References

- Ardakani, A., Bayat, M. and Javanmard, M. (2014), "Numerical modeling of soil nail walls considering mohr coulomb, hardening soil and hardening soil with small-strain stiffness effect models", *Geomech.*

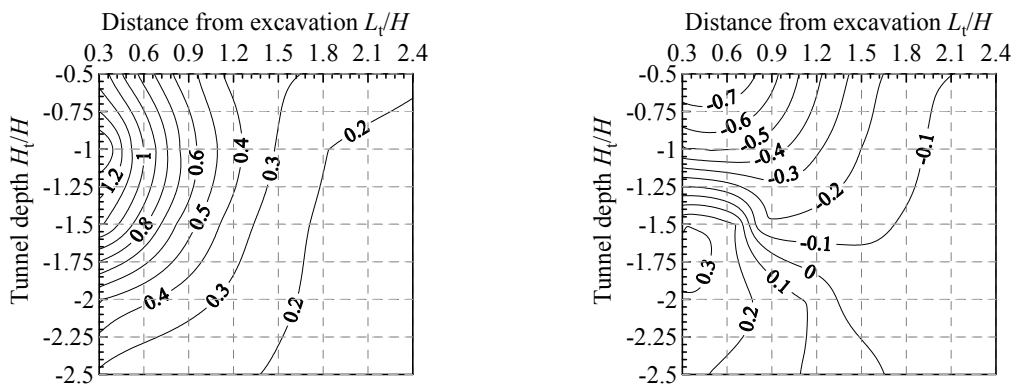
- Eng., Int. J.*, **6**(4), 391-401.
- Bousbia, N. and Messast, S. (2015), "Numerical modeling of two parallel tunnels interaction using three-dimensional Finite Elements Method", *Geomech. Eng., Int. J.*, **9**(6), 775-791.
- Burford, D. (1986), "Heave of tunnels beneath the Shell Centre, London, 1956-1986", *Geotechnique*, **38**(1), 155-157.
- Chang, C.T., Sun, C.W., Duann, S.W. and Hwang, R.N. (2001a), "Response of a Taipei Rapid Transit System (TRTS) tunnel to adjacent excavation", *Tunn. Undergr. Sp. Tech.*, **16**(3), 151-158.
- Chang, C.T., Wang, M.J., Chang, C.T. and Sun, C.W. (2001b), "Repair of displaced shield tunnel of the Taipei rapid transit system", *Tunn. Undergr. Sp. Tech.*, **16**(3), 167-173.
- Do, N.A., Dias, D., Djeran-Maigre, I. and Oreste, P. (2014), "2d numerical investigations of twin tunnel interaction", *Geomech. Eng., Int. J.*, **6**(3), 263-275.
- Doležalová, M. (2001), "Tunnel complex unloaded by a deep excavation", *Comput. Geotech.*, **28**(s6-7), 469-493.
- Hu, Z.F., Yue, Z.Q., Zhou, J. and Tham, L.G. (2003), "Design and construction of a deep excavation in soft soils adjacent to the Shanghai Metro tunnels", *Can. Geotech. J.*, **40**(5), 933-948.
- Huang, X., Schweiger, H.F. and Huang, H. (2011), "Influence of Deep Excavations on Nearby Existing Tunnels", *Int. J. Geomech.*, **13**(2), 170-180.
- Huang, X., Zhang, D.M. and Huang, H.W. (2014), "Centrifuge modelling of deep excavation over existing tunnels", *P. I. Civil Eng-GeoTec*, **167**(GE1), 3-18.
- Hwang, R.N., Duann, S.W., Cheng, K.H. and Chen, C.H. (2011), "Damages to metro tunnels due to adjacent Excavations", *Proceeding of TC302 Symposium Osaka, International Symposium on Backwards Problem in Geotechnical Engineering and Monitoring of Geo-Construction*, Osaka, Japan, July.
- Kung, G., Hsiao, E. and Juang, C. (2007), "Evaluation of a simplified small-strain soil model for analysis of excavation-induced movements", *Can. Geotech. J.*, **44**(6), 726-736.
- Lee, K.M. and Ge, X.M. (2001), "The equivalence of a jointed shield driven tunnel lining to a continuous ring structure", *Can. Geotech. J.*, **38**(3), 461-483.
- Liu, H., Li, P. and Liu, J. (2011), "Numerical investigation of underlying tunnel heave during a new tunnel construction", *Tunn. Undergr. Sp. Tech.*, **26**(2), 276-283.
- Ng, C.W.W., Shi, J. and Hong, Y. (2013), "Three-dimensional centrifuge modelling of basement excavation effects on an existing tunnel in dry sand", *Can. Geotech. J.*, **50**(8), 874-888.
- Ng, C.W.W., Sun, H.S., Lei, G.H., Shi, J.W. and Mašin, D. (2015a), "Ability of three different soil constitutive models to predict a tunnel's response to basement excavation", *Can. Geotech. J.*, **52**(11), 1685-1698.
- Ng, C.W.W., Shi, J., Mašin, D., Sun, H. and Lei, G.H. (2015b), "Influence of sand density and retaining wall stiffness on three-dimensional responses of tunnel to basement excavation", *Can. Geotech. J.*, **52**(11), 1811-1829.
- Richards, J.A. (1998), "Inspection, maintenance and repair of tunnels, International lessons and practice", *Tunn. Undergr. Sp. Tech.*, **13**(4), 369-375.
- Sharma, J.S., Hefny, A.M., Zhao, J. and Chan, C.W. (2001), "Effect of large excavation on deformation of adjacent MRT tunnels", *Tunn. Undergr. Sp. Tech.*, **16**(2), 93-98.
- Simpson, B. (1992), "Retaining structure-displacement and design (32nd Rankine Lecture)", *Géotechnique*, **42**(4), 541-576.
- The British Tunneling Society (2006), *The Joint Code of Practice for Risk Management of Tunnel Works*; The International Tunneling Insurance Group (ITIG), British.
- Zhang, J., Chen, J., Wang, J. and Zhu, Y. (2013), "Prediction of tunnel displacement induced by adjacent excavation in soft soil", *Tunn. Undergr. Sp. Tech.*, **36**(2), 24-33.
- Zheng, G. and Li, Z.W. (2012), "Comparative analysis of responses of buildings adjacent to excavations with different deformation modes of retaining walls", *Chinese J. Geotech. Eng.*, **34**(6), 970-977.
- Zheng, G. and Wei, S.W. (2008), "Numerical analyses of influence of overlying pit excavation on existing tunnels", *J. Cent. South Univ.*, **15**(S2), 69-75.
- Zheng, G., Wei, S.W., Peng, S.Y., Diao, Y. and Ng, C.W.W. (2010), "Centrifuge modeling of the influence

of basement excavation on existing tunnel”, *Proceedings of the 7th International Conference on Physical Modeling in geotechnics*, Zurich, Switzerland, June.

CC

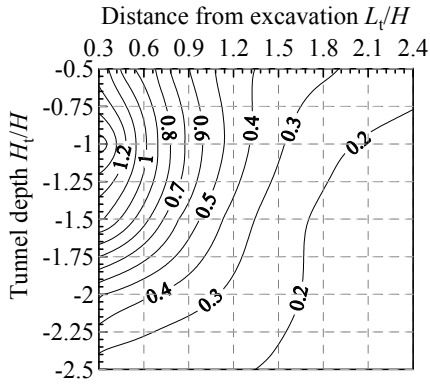
Appendix A
Design charts for the estimation of normalized displacements of tunnels adjacent to excavations

Design charts to estimate the normalized displacements of tunnels adjacent to excavations with different horizontal displacements of the retaining structure (denoted as $x\%H$) and different deformation modes are illustrated below. The unit of these contours is $\%H$.

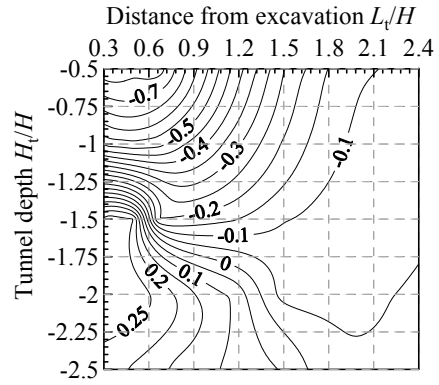


(a) Horizontal displacement contour (unit: $\%H$) (b) Vertical displacement contour (unit: $\%H$)

Fig. A1 Convex-type deformation with $0.167\%H$

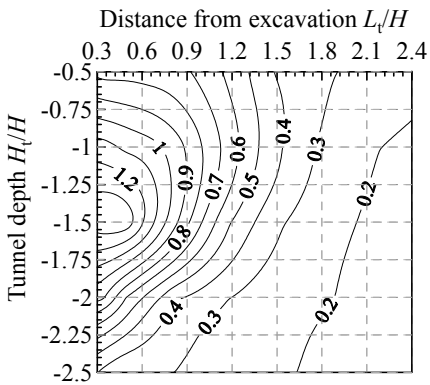


(a) Horizontal displacement contour (unit: %H)

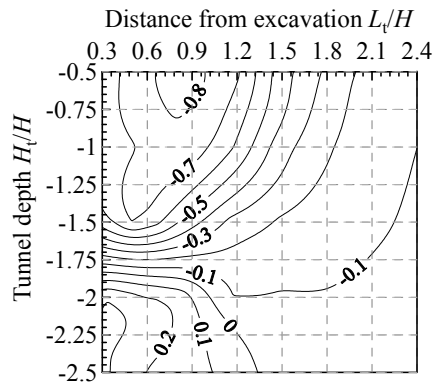


(b) Vertical displacement contour (unit: %H)

Fig. A2 Composite-type deformation with 0.167%H

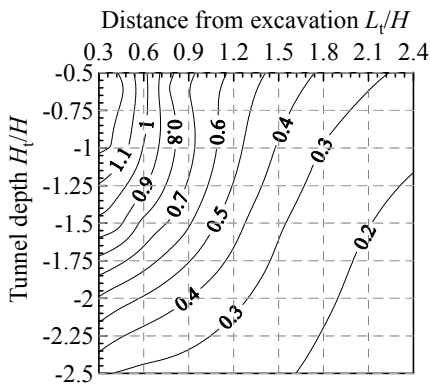


(a) Horizontal displacement contour (unit: %H)

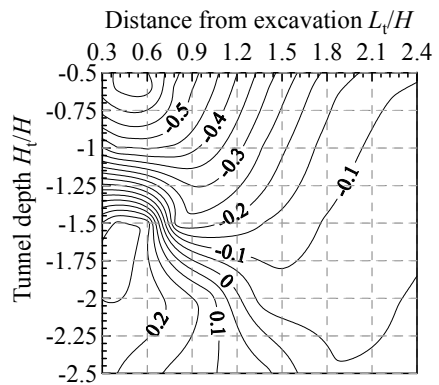


(b) Vertical displacement contour (unit: %H)

Fig. A3 Kick-in-type deformation with 0.167%H



(a) Horizontal displacement contour (unit: %H)



(b) Vertical displacement contour (unit: %H)

Fig. A4 Cantilever-type deformation with 0.167%H

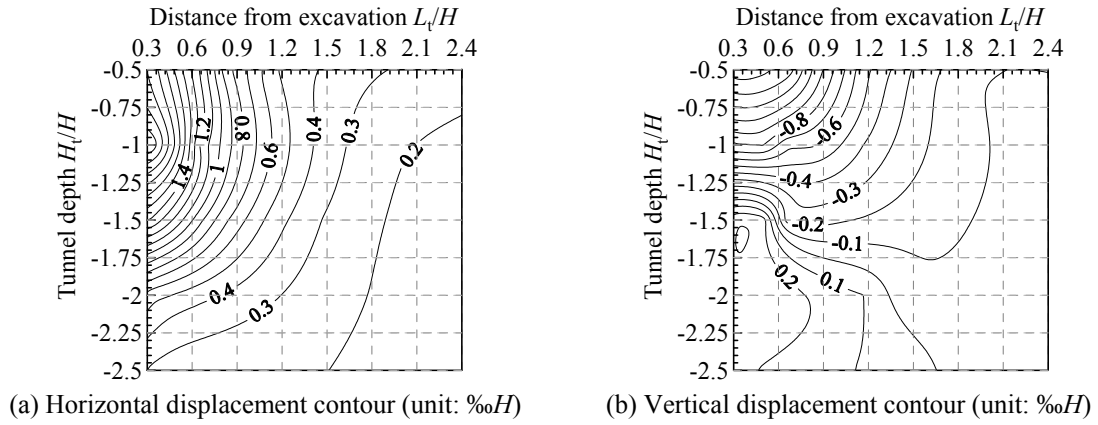


Fig. A5 Convex-type deformation with 0.25%*H*

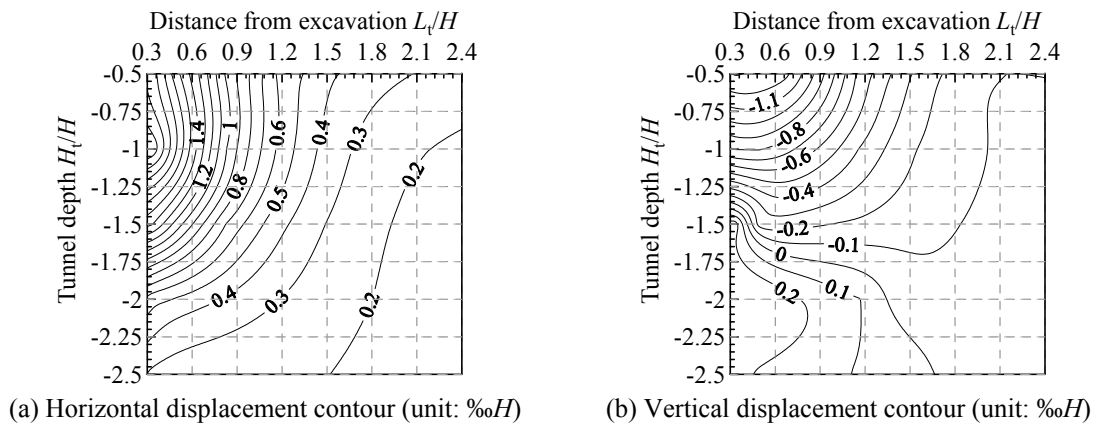


Fig. A6 Composite-type deformation with 0.25%*H*

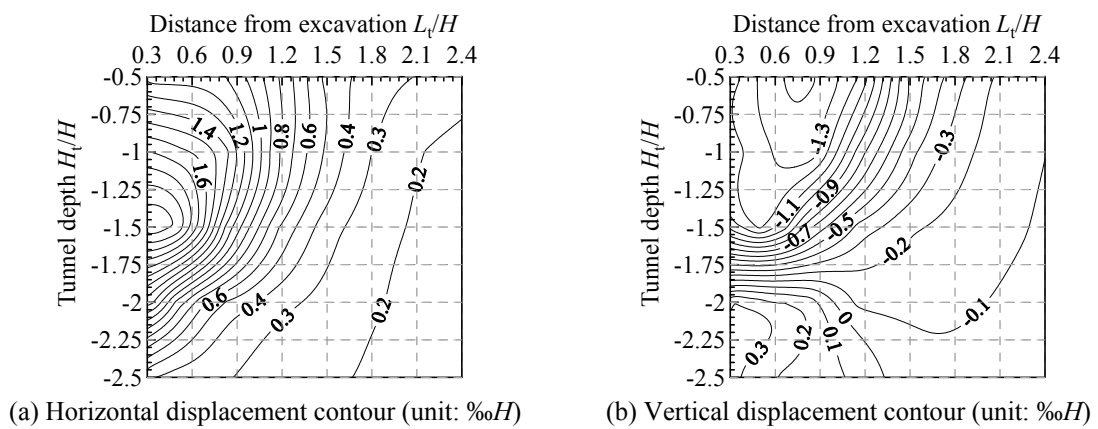
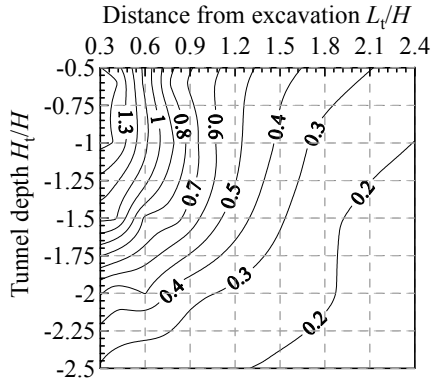
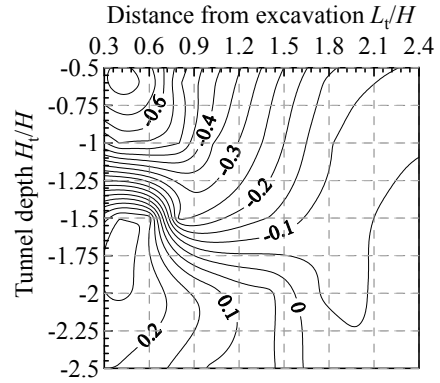


Fig. A7 Kick-in-type deformation with 0.25%*H*

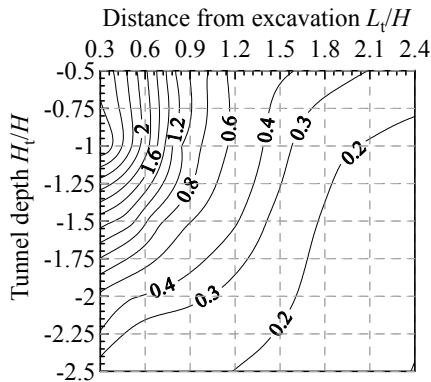


(a) Horizontal displacement contour (unit: %H)

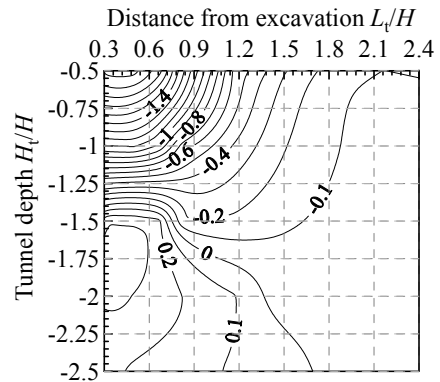


(b) Vertical displacement contour (unit: %H)

Fig. A8 Cantilever-type deformation with 0.25%H

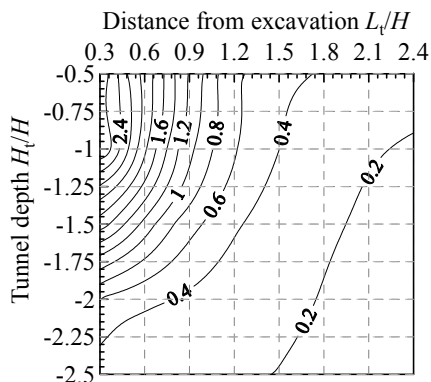


(a) Horizontal displacement contour (unit: %H)

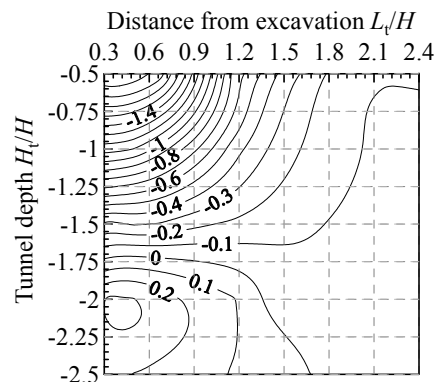


(b) Vertical displacement contour (unit: %H)

Fig. A9 Convex-type deformation with 0.333%H



(a) Horizontal displacement contour (unit: %H)



(b) Vertical displacement contour (unit: %H)

Fig. A10 Composite-type deformation with 0.333%H

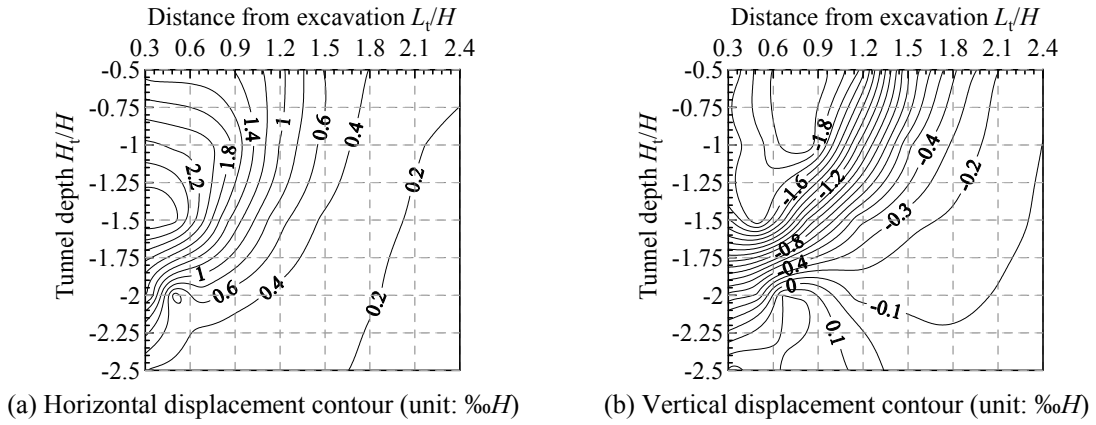


Fig. A11 Kick-in-type deformation with 0.333‰H

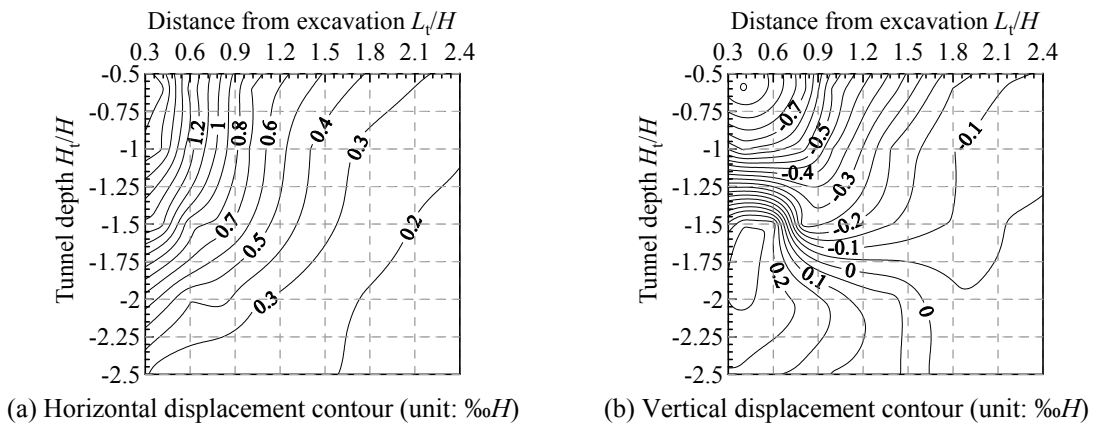


Fig. A12 Cantilever-type deformation with 0.333‰H

Appendix B
Design table to determine the influence zones of
the excavation on an adjacent tunnel

Table B1 Design table of influence zones of the excavation on an adjacent tunnel

Excavation depth H	Horizontal displacement of the retaining structure δ_{hmax}	Deformation mode	Control value: 20 mm (very severe influence zone)			Control value: 10 mm (severe influence zone)			Control value: 5 mm (moderate influence zone)		
			L	V_1	V_2	L	V_1	V_2	L	V_1	V_2
12 m	20 mm (0.167% H)	Convex				0.83	1.30	1.57	1.50	1.73	2.14
		Composite				0.85	1.30	1.59	1.40	1.73	2.14
		Cantilever				0.24	0.38	0.46	1.33	1.53	2.02
		Kick-in				0.93	1.67	1.96	1.46	1.86	2.37
	30 mm (0.25% H)	Convex	0.63	1.00	1.29	1.00	1.39	1.81	1.60	1.65	2.20
		Composite	0.60	1.00	1.13	1.04	1.39	1.81	1.61	1.65	2.20
		Cantilever				0.72	1.14	1.38	1.39	1.50	2.05
		Kick-in				1.19	1.62	2.10	1.60	1.85	2.42
	40 mm (0.333% H)	Convex	0.70	1.09	1.34	1.03	1.42	1.80	1.55	1.73	2.21
		Composite	0.69	1.09	1.24	1.06	1.42	1.82	1.60	1.73	2.21
		Cantilever				0.80	1.21	1.45	1.46	1.62	2.05
		Kick-in	0.67	1.01	1.27	1.26	1.73	2.15	1.64	1.86	2.47
15 m	25 mm (0.167% H)	Convex	0.48	1.05	1.16	0.94	1.53	1.83	1.50	1.92	2.35
		Composite	0.48	1.07	1.15	1.00	1.55	1.86	1.80	1.83	2.35
		Cantilever				1.00	1.46	1.86	1.80	1.86	2.40
		Kick-in				1.13	1.57	2.25	1.76	2.10	2.80
	37.5 mm (0.25% H)	Convex	0.55	1.08	1.23	1.07	1.63	1.92	1.70	1.97	2.43
		Composite	0.57	1.08	1.30	1.10	1.55	1.93	1.80	1.84	2.43
		Cantilever	0.46	1.02	1.09	1.06	1.47	1.90	1.80	1.85	2.46
		Kick-in	0.76	1.61	1.83	1.35	1.71	2.34	1.80	2.11	2.90
	49.5 mm (0.333% H)	Convex	0.93	1.33	1.72	1.34	1.53	2.09	2.00	1.87	2.46
		Composite	0.95	1.38	1.73	1.36	1.54	2.10	2.00	1.91	2.48
		Cantilever	0.60	1.10	1.32	1.13	1.50	2.00	1.87	1.85	2.51
		Kick-in	1.20	1.53	1.95	1.50	1.72	2.40	1.89	2.12	3.00
18 m	30 mm (0.167% H)	Convex	0.54	1.42	1.50	1.08	1.61	1.93	2.00	1.97	2.45
		Composite	0.58	1.50	1.55	1.10	1.66	2.00	2.10	2.00	2.50
		Cantilever				0.80	1.50	1.70	1.80	1.66	2.48
		Kick-in	0.72	1.66	1.78	1.40	1.77	2.28	2.10	1.97	2.60

Table B1 Design table of influence zones of the excavation on an adjacent tunnel

Excavation depth H	Horizontal displacement of the retaining structure δ_{hmax}	Deformation mode	Control value: 20 mm (very severe influence zone)			Control value: 10 mm (severe influence zone)			Control value: 5 mm (moderate influence zone)		
			L	V_1	V_2	L	V_1	V_2	L	V_1	V_2
			45 mm (0.25% H)	Convex	0.80	1.50	1.65	1.20	1.70	1.98	2.00
Composite	0.81	1.53		1.68	1.28	1.68	2.00	2.10	2.00	2.56	
Cantilever	0.40	0.62		0.68	1.00	1.32	1.82	2.00	1.26	2.50	
Kick-in	1.20	1.42		2.07	1.53	1.51	2.42	2.20	2.20	2.90	
60 mm (0.333% H)	Convex	1.00	1.32	1.73	1.37	1.50	2.00	2.20	2.00	2.55	
	Composite	1.08	1.36	1.78	1.40	1.54	2.10	2.24	2.06	2.60	
	Cantilever	0.60	1.00	1.15	1.20	1.47	1.88	2.00	1.66	2.50	
	Kick-in	1.40	1.44	2.11	1.70	1.77	2.50	2.30	2.00	2.84	